Synergistic aircraft and ground observations of transported wildfire smoke and its impact on air quality in New York City during the summer 2018 LISTOS campaign

Yonghua Wu [1, 2*], Amin Nehrir [3], Xinrong Ren [4, 5], Russell R. Dickerson [4], Jianping Huang [6], Phillip R. Stratton [4], Guillaume Gronoff [3, 7], Susan Kooi [3, 7], James Collins [3, 7], Timothy A. Berkoff [3], Liqiao Lei [3, 8], Barry Gross [1, 2], Fred Moshary [1, 2]

[1] City College of New York, New York, NY 10031, USA
[2] NOAA – Cooperative Science Center for Earth System Sciences and Remote Sensing Technologies
[3] NASA Langley Research Center, Hampton, VA 23681, USA
[4] Department of Atmospheric and Oceanic Science, University of Maryland, College Park, MD 20742, USA
[5] Air Resources Laboratory, National Oceanic and Atmospheric Administration (NOAA), College Park 20742, MD, USA
[6] NOAA/NCEP/ Environmental Modeling Center and I.M. System Group, College Park, MD 20740, USA
[7] Science Systems Applications, Inc., Hampton, VA 23666, USA
[8] Universities Space Research Association, Columbia, MD 21046, USA
[*]Correspondence to yhwu@ccny.cuny.edu

ABSTRACT Air pollution associated with wildfire smoke transport during the summer can significantly affect ozone (O_3) and particulate matter (PM) concentrations, even in heavily populated areas like New York City (NYC). Here, we use observations from aircraft, ground-based lidar, in-situ analyzers and satellite to study and assess wildfire smoke transport, vertical distribution, optical properties, and potential impact on air quality in the NYC urban and coastal areas during the summer 2018 Long Island Sound Tropospheric Ozone Study (LISTOS). We investigate an episode of dense smoke transported and mixed into the planetary boundary layer (PBL) on August 15-17, 2018. The horizontal advection of the smoke is shown to be characterized with the prevailing northwest winds in the PBL (velocity>10 m/s) based on Doppler wind lidar measurements. The wildfire sources and smoke transport paths from the northwest US/Canada to northeast US are identified from the NOAA hazard mapping system (HMS) fires and smoke product and NOAA-HYbrid Single Particle Lagrangian Integrated Trajectory (HYSPLIT) backward trajectory analysis. The smoke particles are distinguished from the urban aerosols by showing larger lidar-ratio (70-sr at 532-nm) and smaller depolarization ratio (0.02) at 1064-nm using the NASA High Altitude Lidar Observatory (HALO) airborne high-spectral resolution lidar (HSRL) measurements. The extinction-related angstrom exponents in the near-infrared (IR at 1020-1640 nm) and Ultraviolet (UV at 340-440 nm) from NASA-Aerosol Robotic Network (AERONET) product show a reverse variation

trend along the smoke loadings, and their absolute differences indicate strong correlation with the smoke-Aerosol Optical Depth (AOD) (R>0.94). We show that the aloft smoke plumes can contribute as much as 60~70% to the column AOD and that concurrent high-loadings of O_3, carbon monoxide (CO), and black carbon (BC) were found in the elevated smoke layers from the University of Maryland (UMD) aircraft in-situ observations. Meanwhile, the surface $PM_{2.5}$ (PM with diameter ≤ 2.5 μm), organic carbon (OC) and CO measurements show coincident and sharp increase (e.g., $PM_{2.5}$ from 5 μg/m^3 before the plume intrusion to ~30 μg/m^3) with the onset of the plume intrusions into the PBL along with hourly O_3 exceedances in the NYC region. We further evaluate the NOAA- National Air Quality Forecasting Capability (NAQFC) model PBL-height, $PM_{2.5}$, and O_3 with the observations and demonstrate good consistency near the ground during the convective PBL period, but significant bias at other times. The aloft smoke layers are sometimes missed by the model.

Key words: Wildfire smoke, ozone, $PM_{2.5}$, black carbon, organic carbon, optical properties

1. Introduction

The frequency and intensity of wildfire events in the western United States (US) and Canada are expected to increase because of global changes in temperature, humidity, wind and rain patterns caused by climate change (Dennison et al., 2014; Schoennagel et al., 2017). This is critical for air quality since wildfires can emit large amounts of particulate matter (PM) and gaseous compounds, i.e. OC, BC, CO, carbon dioxide (CO_2), nitrogen oxides (NOx), and volatile organic compounds (VOCs), etc. (Andreae et al., 1988; Crutzen et al., 1979; Liu et al., 2014). The emissions of smoke particles and O_3 precursors can result in $PM_{2.5}$ (PM with diameter ≤ 2.5 μm) and O_3 exceedance of the national ambient air quality standard (NAAQS) in down-wind areas (Colarco et al., 2004; Dreessen et al., 2016; Jaffe et al., 2012, 2013; Sapkota et al., 2005; Taubman et al., 2004). Most importantly, during long-range transport of wildfire smoke, the plume can change its chemical composition and potentially affects air quality on local and regional scales when entrained down into the planetary boundary layer (PBL).

Satellite remote sensing has been extensively used to identify these wildfires source and track smoke transport, but this tool is generally limited to column or altitude-integrated total amounts (Hoff et al., 2009). Meanwhile, routine air quality monitoring by U.S. Environmental Protection Agency (EPA) or associated state agencies is mostly deployed at the near-ground and these monitoring networks are

generally sparse due to costs involved. Unfortunately, there is distinct difficulty in attempting to correlate and interpret satellite column measurement with EPA surface-level routine monitoring, i.e., vertical distribution and aerosol type (Crawford et al., 2014; Hoff et al., 2009). For instance, aloft aerosol plumes might contribute to total AOD measured from satellite sensors, but have no connection with ground $PM_{2.5}$. In addition, different type of aerosols show different optical properties that affect AOD dramatically, but may have similar mass concentration. For smoke particles in general, another gap is the optical-mass conversion between satellite retrieved AOD and surface $PM_{2.5}$ concentration, which is related to aerosol microphysics and chemical properties. Thus, vertical distributions and spatiotemporal variations of aerosols and their types (optical properties) are critical to satellite remote sensing application to air quality (Hoff et al., 2009, Han et al., 2015, Li et al., 2016, Lin et al., 2015, Liu et al., 2011, Zhang et al., 2015).

On the other hand, Chemical Transport Models (CTM) and air quality models such as the Community Multiscale Air Quality modeling (CMAQ) have been extensively used to evaluate smoke impacts (Dreessen et al., 2016), but there are large uncertainties on wildfire emission inventories and fire magnitude, fuel type and complex meteorology-chemistry processes (National Research Council, 2009). In addition, the injection height of the smoke plumes is also critical to predict the range-resolved transport of the smoke that also can affect the potential mixing down into PBL and near ground. Thus, smoke from wildfires or biomass burning may cause uncertainty in air quality model forecast except the influences from meteorological factors and emission inventories. Many efforts have been made to improve modeling the impacts of wildfire emissions on air quality (Lee et al., 2016).

It is generally difficult in validation studies to quantify smoke contribution to air quality (e.g., ground-level $PM_{2.5}$) via long-distance transport because of the resultant unavoidable mixture of smoke with other air mass. It is also a challenge to distinguish the transported wildfire smoke from local urban aerosols in the PBL based on their size information since both are fine-mode dominated and mixed. The wildfire smoke transport may result in the “exceptional” events of more severe air quality exceedances, which is beyond local air quality management and emission control (Jaffe et al., 2013; Dreessen et al.,

2016; Wu et al., 2017, 2018). The episodes of wildfire smoke transport and aerosol vertical distribution have been observed from CCNY-lidar in the NYC area (Chillrud et al., 2019; Wu et al., 2012, 2016 and 2018), but there is a lack of regional-scale and gaseous compounds observations, specifically their vertical distribution, smoke discrimination from the urban aerosols, and potential effects on O_3 exceedance of NAAQS to interpret these events properly.

While we have focused on $PM_{2.5}$, the formation and transport of O_3 within these plumes is an additional air quality factor that is critical to human health. Ozone exceedance of the NAAQS (70 ppb daily maximum 8-hr mean) and haze events frequently occur during the summer in NYC and its downwind coastal areas such as the Long Island Sound (Miller, et al., 2017). Such pollution episodes are generally related to urban emissions of pollutants, photochemical and chemical transformation, smoke plume transport, and urban-coast meteorology. However, there is lack of observations of vertical distribution of O_3, $PM_{2.5}$ and their precursors, and meteorological parameters for better understanding the high O_3 formation - and model forecast performance. To address this important issue, the Long Island Sound Tropospheric Ozone Study (LISTOS) campaign was launched in the summer of 2018 to observe and understand the regional-scale high O_3 events in Long Island Sound (Miller, 2017, https://www.nescaum.org/documents/listos). The measurements were made from ground-based sites, research aircraft, marine vessels, and satellite observations in Long Island Sound where a land–sea breeze feature often leads to high O_3 concentrations along the Connecticut shoreline (see more logistic information in Karambelas (2020)).

During the LISTOS campaign, an opportunity of synergistic measurements occurs to better understand wildfire smoke optical properties from remote sensing observations and its impact to the air quality. In this study, we present wildfires smoke optical characteristics, time-height distribution, and potential impact on the air quality in NYC and Long Island Sound during August 15-17, 2018. The observations include the NASA HALO, a combined Differential Absorption Lidar (DIAL) and HSRL, the UMD aircraft in-situ samplers, ground-based wind, aerosol and O_3 lidars and the surface samplers by the New York State Department of Environment Conservation (NYSDEC). The NOAA-NAQFC model

forecast products were assessed during the 2018 LISTOS summer campaign. The goals of this study are to 1) characterize regional-scale smoke vertical distribution, optical properties, gaseous compounds, and the smoke particles discrimination from urban aerosols; 2) assess smoke impacts on local air quality; and 3) assess model forecast product of PBL-height (PBLH), ground $PM_{2.5}$ and O_3. To allow us to separate the different aerosol layers throughout the troposphere, the time-height distribution of aerosol optical properties are presented to identify the intrusions of smoke plumes and mixing into the PBL, and distinguish the smoke particles from local urban aerosols. Regional-scale vertical distribution of smoke-associated particles and gaseous compounds are demonstrated from the NASA HALO instrument and UMD aircraft observations. The temporal variations and the correlation analysis of ground $PM_{2.5}$, OC, BC, CO and O_3 are analyzed to evaluate the smoke impacts. Finally, using the remote sensing and in-situ data, we evaluate the NAQFC product of O_3, $PM_{2.5}$ and PBLH. This paper is organized as follows. In Section 2, the observation methods and data are described. In Section 3, the results and discussions on the smoke aerosols, as well as the variations of ground $PM_{2.5}$ and chemical species are presented. Finally, Section 4 summarizes the conclusions.

2. Observation Methodology and Data

2.1 Ground-based observation

Table-1 lists the ground-site coordinates and the data used in this study. At the City College of New York (CCNY)-site (40.820° N, 73.949° W), the remote sensing instrument suite includes a 3-wavelength elastic (Mie)-Raman lidar, a ceilometer (Vaisala CL-51), an AERONET (Aerosol Robotic Network) Cimel sun/sky radiometer, and a coherent Doppler wind lidar (Leosphere Windcube 200S). Meanwhile, a standard surface air quality monitoring station is operated by the NYSDEC on the CCNY campus for $PM_{2.5}$, O_3 and CO measurements. There is another AERONET site at Brookhaven National Laboratory (BNL, 40.866º N, 72.885º W) in Upton, NY (~90 km to the southeast of the CCNY-site). Figure 1 shows the locations of select ground stations used in this study.

The CCNY-lidar transmits three wavelengths (1064-, 532- and 355-nm) and uses a receiver telescope (Ø50-cm) collecting three elastic scattering and two Raman-scattering returns by nitrogen and

142 water vapor molecules excited by the 355-nm laser output (Wu et al., 2009). It is generally operated
143 during daytime on weekdays with an observer due to the eye-safety concerns. The multi-wavelength
144 configuration can be used to obtain extinction-related Angstrom exponent (EAE) that help distinguish
145 fine mode (smoke and industrial aerosol) from coarse mode particles (dust, sea salt and cloud). Generally,
146 fine mode particles show larger EAE while coarse mode particles indicate smaller EAE (Eck et al., 1999).
147 The strong signal-to-noise ratios (SNR) of the lidar allow us to measure aloft aerosol plumes and retrieve
148 aerosol extinction and backscatter profiles in the troposphere (Su et al., 2013, 2014). In addition, the
149 ceilometer (Vaisala CL-51) measures aerosol backscatter at a laser wavelength of 910 nm with a vertical
150 range resolution of 10 m (Gan et al., 2011). The measured attenuated backscatter coefficient profiles can
151 be used to determine PBLH and residual layer height. According to Stull (1988), a convective boundary
152 layer (CBL) that occurs during the daytime is usually referred to as a mixing layer; during this period, the
153 mixing layer height (MLH) represents PBLH. After the sunset, the surface cooling creates a stable
154 (nocturnal) boundary layer, above which is a residual layer, leftover from the daytime mixed layer. The
155 PBLH or MLH can be detected from the ceilometer and lidar based on vertical gradient variation of
156 aerosol backscatter profiles (Menut et al., 1999; Davis et al. 2000, Brook et al. 2003, Haeffelin et al.,
157 2012, Scarino et al. 2014). In this study, a wavelet analysis technique is used to locate the absolute
158 maximum negative gradient of attenuated backscatter profile that is defined as the PBLH (Gan et al.,
159 2011). Furthermore, a quality control of the PBLH estimate is performed which includes cloud screening,
160 temporal continuity, and screening of an aloft or residual layer during the night and early-morning. Thus,
161 one can obtain boundary layer information as well as residual-layer height, aerosol-cloud discrimination,
162 and optical properties of aerosols and clouds from the CCNY-lidar measurement (Wu et al., 2009, 2018).
163 On the other hand, the CIMEL sunphotometers (part of the NASA AERONET) at CCNY and BNL
164 provide column aerosol optical depth (AOD), extinction Angstrom exponent (EAE), and microphysical
165 parameters (volume size distribution, refractive index and single-scattering albedo (SSA)) (Holben et al.,
166 1998). The sunphotometer-measured AOD is used to constrain the lidar-ratio or aerosol extinction-to-
167 backscatter ratio for retrieving aerosol extinction and backscatter profiles in the free troposphere (Wu et

al., 2012); and its value depends on aerosol optical properties and can help classify aerosol types (Burton et al., 2013). Absorbing Angstrom exponent (AAE) can be simulated from the AERONET inversions that indicates the light absorbing component of OC known as "brown carbon" (BrC) for smoke (Mok et al., 2016).

In addition, a coherent Doppler Wind Lidar (Leosphere WindCube 100s) was deployed to measure wind profiles in Bronx (Lehman College, 40.873° N, 73.894° W, 7.5 km to the NE of CCNY) as part of the NYS-Mesonet (Brotzge et al., 2020). The wind lidar uses a vertically-pointing eye-safe laser (wavelength 1.54 μm with a repetition rate of 10 kHz) to estimate wind velocities, and a scanning sequence (Doppler beam swinging with elevation angle 75 deg at North, East, South and West) to obtain horizontal wind velocity and direction. All data are collected, quality-controlled, and archived. The lidar has a range-gate spacing of 25-50 m and time resolution less than 10 seconds. Intensity of the turbulence can be characterized by variance of vertical velocity '*w*' at an interval of a few minutes (Tucker et al., 2009). The turbulence-based PBLH or MLH can be calculated from variance of vertical velocity with a threshold method (e.g. 0.15 m/s^2 in this study) (Schween et al., 2014).

The NASA Langley Mobile Ozone Lidar (LMOL) is a ground-based tropospheric profiling ozone lidar system, housed in a mobile trailer, and has participated in air quality studies since 2014 and is part of the NASA-sponsored Tropospheric Ozone Lidar Net-work (http://www air.larc.nasa.gov/missions/TOLNet/). The technical details and detection precision are given in multiple references (Young et al., 2017, Gronoff et al., 2019, Farris et al., 2019). LMOL was deployed at Sherwood Island Park, Westport, CT (73.337° W, 41.118° N, 2.5-meter ASL) to measure ozone vertical profiles using a differential absorption principle at the UV wavelength pair of 287 and 292 nm. Ozone cross sections along with pressure and temperature information are used as part of the process to extract ozone mixing ratio as a function of altitude. The process is repeated for each new profile on a 5–10 min temporally averaged basis, to provide a continuous curtain display on the evolution of ozone vertical distribution during the course of a day. Estimation of uncertainties follow the standardized procedure

described in Leblanc et al (2018) and optimization of vertical resolution with altitude follows Gronoff et al (2019).

NYSDEC operates monitoring sites to measure O_3, NO_x, $PM_{2.5}$ and $PM_{2.5}$ speciation at the urban, suburban and rural sites in New York (Rattigan et al., 2010, 2016). The locations of ground monitoring stations are shown in Fig.1. Co-located at the CCNY campus, $PM_{2.5}$, O_3, and CO are reported with 1-minute average during the LISTOS campaign. The sites at Queens College (QC, 40.736º N, 73.822º W in the borough of Queens) and IS-52 (located in borough of Bronx) are two Chemical Speciation Network (CSN) trends sites in New York State, where there is an extensive set of ambient monitoring equipment for gaseous and aerosol sampling (e.g. O_3, NO_2, NO, SO_2, CO, $PM_{2.5}$ and its speciation). Hourly OC and EC of $PM_{2.5}$ are measured at QC-site, using a Sunset OC/EC field analyzer (Sunset Lab, Inc.) (Rattigan et al., 2010, 2016). Meanwhile, a two-wavelength Aethalometer (Magee Scientific model AE-21, λ=880 nm and 370 nm) measures BC at the QC-site (Rattigan et al., 2013). The BC measured at the two wavelengths, BC_{UV} (370) and BC_{IR} (880), can help distinguish the BC sources (e.g. biomass burning vs. vehicles) because their difference defined as delta-C (BC_{UV} - BC_{IR}) is large for the organic absorption particles, e.g. biomass burning aerosols (Wang et al., 2012). OC is generally emitted from combustion activities or produced from secondary processes such as gas-to-particle formation. EC, also known as light absorbing carbon or BC, is emitted directly from combustion sources. With the prevailing western and northwest winds, the site at Newburgh (41.499° N, 74.099° W, 83-km away in the north of CCNY) located in the northwest NYC generally represent the upwind rural area of NYC, where the hourly $PM_{2.5}$, CO and BC are observed. The correlation of the pollutants in the urban and upwind rural areas can be an indicator of regional transport (Lall et al., 2006). Further details about these sites can be found at the website (http://www.dec.ny.gov/chemical/8406.html).

2.2 NASA and University of Maryland (UMD) Aircraft observations

The NASA airborne HALO includes a HSRL and H_2O or CH_4- DIAL (Nehrir et al., 2017, 2018). This study uses the HALO airborne HSRL measurements of aerosol extinction at 532 nm and aerosol

backscatter and depolarization at 532 and 1064 nm (Hair et al. 2008, Burton et al., 2013, 2014 and 2015). The spectral dependence of particle depolarization ratio can help classify aerosol types while the lidar-ratio at 532-nm can be directly measured by independently deriving aerosol extinction and backscatter coefficients (Hair et al. 2008, Burton et al., 2015, Haarig et al., 2018). The power of polarization lidar in isolating different particles is that the particle depolarization ratio (PDR) from lidar is a strong indicator of non-spherical particles and is sensitive to the fraction of non-spherical particles and their size. Generally, PDR is smaller for smoke and anthropogenic aerosol due to its spherical shape, but larger for dust particle attributed to its non-spherical shape. Both observations and numerical simulations indicate that smoke particles show larger PDRs at short-wavelength (355, 532 nm) than those at 1064 nm, which might be explained by the presence of coated soot aggregates and smaller particles (Burton et al., 2015, Mishchenko et al., 2016, Haarig et al., 2018). The technical details on the NASA-HSRL measurement approach can be found in Hair et al. (2008).

In addition, the UMD Cessna research aircraft was deployed in the field campaign to measure aerosol optical properties (total scattering and absorption), BC and trace gases (O_3, CO, CO_2, CH_4, NOx, Formaldehyde (HCHO), etc.). Aerosol scattering and absorption coefficients were measured by a 3-wavelength Nepholometer (TSI3563) and a Particle Soot/Absorption Photometer (PSAP), respectively. The aerosol single-scattering-albedo (SSA), a ratio of aerosol total scattering coefficient to the extinction, can be directly estimated from the aircraft observations, which is critical in the aerosol radiative effect. The BC is measured by a 7-wavelength Aethalometer (Magee Scientific AE33, λ=370-950 nm) that provides information of spectral contribution of absorbing aerosol and distinguish BC from BrC (Mok et al., 2016). The data products provide a good opportunity to assess multiple gaseous compounds (O_3 and its precursors), black carbon, aerosol scattering and absorption, and their vertical distribution for this wildfire smoke event in Long Island Sound. The technical details on the instruments and observations can be found in the literatures (Taubman et al., 2004, Castellanos et al., 2011; Ren et al., 2018, 2019).

2.3 NOAA Satellite and model products

The NOAA Hazard Mapping System (HMS) was developed in 2001 by the National Environmental Satellite and Data Information Service (NESDIS) as an interactive tool to identify fires and smoke emissions over North America in an operational environment (Ruminski et al., 2006). The system utilizes two geostationary and five polar orbiting environmental satellites. The result is a quality-controlled display of the locations of fires and significant smoke plumes. HMS's smoke analysis is based on visual classification of plumes using satellite imagery available during the sunlit part of the orbit. The smoke density information is qualitatively described using thin, medium, and thick labels that are assigned based on the apparent thickness (opacity) of the smoke in the satellite imagery. HMS has a number of detection limitations such as clouds hindering detections, no vertical structure information, no quantitative amount or density of smoke, and the approach is only available during daylight. In addition, the NOAA-HYSPLIT model is used to compute air parcel trajectories and model the dispersion and the route of airborne particles (Draxler et al., 1997) and can be used either in a back-trajectory mode to identify sources or in forecast mode. In this study, the HYSPLIT ensemble backward trajectories were generated with the meteorological field from the North American Regional Reanalysis (NARR, 32 km resolution) model that shows substantial improvements in the accuracy of temperature, winds and precipitation compared to the NCEP-DOE Global Reanalysis-2.

The NAQFC was established by NOAA in partnership with the EPA to provide O_3 and $PM_{2.5}$ forecasts. The NOAA Air Resources Laboratory (ARL) and the NCEP develop upgrades for the NAQFC forecasting system, and conduct and evaluate pre-implementation testing (Lee et al., 2016; Huang et al., 2017). The NAQFC consists of the NOAA-NCEP regional operational weather forecasting model, North America Model (NAM) and EPA-CMAQ model. It is designed to provide 2-day model forecasts of O_3 and $PM_{2.5}$ twice per day at the 06 and 12 UTC cycles. For this study, products with spatial resolution of 12 km at the 06 UTC cycle are used. The NAQFC performs incremental tests and evaluations against the U.S. EPA AIRNow surface monitoring network. A modified version of the U. S. EPA CMAQ v5.0.2 (Foley et al., 2010), is run at 12-km horizontal grid spacing with a Lambert Conformal Conic (LCC) map projection for the product used in this study. The emissions from wildfires, prescribed agricultural burns,

and land clearing fires were computed using the dynamic fire emission modeling U.S. Forest Service BlueSky smoke emission package (O'Neill et al., 2009) and the NOAA-HMS for fire locations and strength.

The NAQFC CMAQv5.0.2 follows largely the U.S. EPA Aero4 module and the related emission and removal processes found in the U.S. EPA-CMAQ version 5.0.2. Gas to particle conversion, heterogeneous reactions, depositional growth, and coagulation are included (Kelly et al., 2009). The Mellor Yamada Janjic (MYJ) PBL scheme (Janjie et al., 2001) is used in this version of NAM. The detailed configuration for NAQFC simulations can be found in Lee et al. (2016).

3. Results and Discussion

3.1 Wildfire smoke sources and transports

Figure 2 shows the wildfire sources and smoke transport from the NOAA-HMS product on Aug.16, 2018. The wildfires occurred in the Northwest U.S. and Western Canada; the continental transport of wildfire smoke (color shading in Fig.2 (a)) can be clearly seen. In Fig.2 (a), the color shadings qualitatively represent the smoke density information. The green shadings correspond to thin density smoke, the yellow shadings to medium density smoke, and the red shadings to thick density smoke. The HYSPLIT ensemble backward trajectories ending at 3-km altitude (plume height from CCNY-lidar observation in Fig.3 (a)) at 15:00 UTC of Aug.16 indicate that these plumes were transported from the wildfire regions in the Northwest U.S. and western Canada. The air traveled for 168-hr (7-day) long from the Pacific Northwest to NYC area, and the air parcel heights are generally above the PBL (>2-km). In addition, high AOD measured by the Visible Infrared Imaging Radiometer Suite (VIIRS) instrument on Suomi-NPP and JPSS-1 indicates heavy loadings of aerosol particles and the transport path to the northeastern US (Fig.2(b)). More optical properties of the plumes will be given in the following Section that can help classify aerosol type. However, an open question is whether these plumes affect the air quality along the transport path. This depends on plume altitudes and how efficiently they mix down into the PBL and reach the surface air.

3.2 Time-height distribution, optical properties of smoke and mixing into the PBL

To address the issue in Section 3.1, Figure 3 gives the time-height distribution of aerosol plumes and PBLH in NYC from the CCNY-lidar and ceilometer measurements. The aloft plume was first observed over NYC in the free troposphere on Aug.15, and the plume heights gradually descended and mixed into the PBL at 17:00 in the afternoon of Aug.15. On the following day (Aug.16), there were multiple layers of dense aerosols between 1-km and 5-km altitude, with the plumes mixed into the PBL at around 15:00 assisted by the simultaneous increase in PBL-height. Some low broken clouds appeared in the PBL-top in the afternoon of Aug.16 marking a haze layer transition. This was further confirmed by the continuous observations from the ceilometer (CL-51). Following this episode through, the enhanced aerosol backscatter intensities in the near surface and PBL are clearly demonstrated during Aug.15-17, 2018. The low PBL-heights in the morning and night of Aug.16 and 17 trap more aerosols near-surface thus showing stronger backscatter intensity. The aerosol plumes are indicated below 2-km before 7:00 on Aug.16 and Aug. 17, which might be entrained into PBL after sunrise when the PBL vertical mixing become stronger.

The horizontal and vertical wind measurements near the CCNY-site are shown in Fig.4. Strong northwest winds (velocity V>10 m/s) were indicated to drive the smoke transport in the PBL and free troposphere on Aug.15 and 16. The horizontal wind velocity in the PBL became lighter from the afternoon of Aug.16 to the morning of Aug.17. Strong vertical convection or turbulence is indicated by the large variance of vertical velocity at noon-time and early afternoon. The mixing-layer-heights (MLHs) are estimated, and the results indicate good correlation with the ceilometer-measured MLHs (R=0.74). In addition, Hung et al. (2020) indicate that PBL entrainment and vertical mixing provide favorable meteorological conditions for the aloft smoke mixing in the PBL in NYC area.

The time-height distribution of aerosol optical properties from the CCNY-lidar retrievals is given in Fig.5. The aerosol extinction coefficients and lidar-ratios are constrained with the co-located AERONET AOD data when the sky is sufficiently cloud free. The AOD from the aloft plumes, PBL

aerosols and total aerosols (< 8 km altitude) can be segmented from the lidar-derived aerosol extinction profile when the aloft plume can be isolated from the PBL. We assume that the aerosols above 8-km altitude can be ignored to the total AOD. First, the aerosol extinction coefficients indicate the aloft dense smoke above 1-km altitude and mixing into the PBL at noon. High Angstrom exponent (>1.5) indicates the fine-mode dominant aerosols in the plume layer in Fig.5 (b). In particular, the AOD from the aloft smoke plume, PBL and total aerosols are estimated at 11:00-16:00 when the aloft plume layers can be isolated from the PBL. In this case, the ratios of plume-AOD to total-AOD indicate that the aloft plume contributes up to 70% of the total AOD. However, this method is difficult to estimate the smoke contribution when the plumes mix into PBL or mix with anthropogenic aerosols during the transport process. The column-average lidar-ratios are 78.5 ± 6.4 sr at 532-nm and 56.9 ± 7.5 sr at 1064-nm, respectively, which are typical values for the smoke aerosols (Burton et al., 2013).

Meanwhile, to get a better sense of other potential high O_3 formation process besides normal PBL chemistry leading to high O_3 surface levels, the vertical distribution of O_3 presented in Fig.6 was measured by the NASA LMOL O_3 lidar system located at Westport, CT, a coastal site along Long Island Sound. Remarkably, concurrent high concentrations of O_3 were observed in the aloft plume layers, showing the values above 70 ppb from the morning to the afternoon on Aug.15 and 16. A similar descending trend of aloft O_3 layer height was shown on Aug.16, along some dispersion or turbulent mixing into the PBL. At altitude below 1.5 km, the O_3 concentrations show a dramatic increase from 40 ppb on Aug.15 to 60 ppb on Aug.16. Such an O_3 increment is likely associated with transported smoke and the local chemical production. We note that there were some low and high clouds on Aug.15-16 as shown in Fig.3. There are no O_3 retrievals below 0.25 km altitude on this particular day due to a temporary instrument issue with the lidar, nor in the low clouds and above 4.5 km in the day due to reduced SNR.

Figure 7 gives the total AOD and Angstrom exponents (AE) at the different wavelength pairs (IR, VIS, and UV) from the AERONET measurements at the CCNY and BNL sites. First, on Aug.15, the AOD shows an increase trend from 0.2 to 0.6 at 532 nm while the AE at VIS (440-870 nm) indicates

large value but slightly temporal variation. However, the AE at the IR pair (1020-1640 nm) indicates a dramatic increase trend whereas the AE at the UV pair (340-440 nm) shows a decrease trend from Aug.15 to Aug.16. Such different variation trends of AE at the IR and UV bands are consistent at two sites; this is associated with smaller particle size and absorption differences at the UV-IR band that are demonstrated with the Mie-scattering simulations. Furthermore, the correlation between the increments of AOD (comparing to the AOD before the smoke intrusion on Aug.15) and AE difference at IR-UV is given in Fig.8. Strong linear correlation (R>0.9 and linear slope at 1.8-2.0) was observed at both two sites, which means that it may be possible to derive a quantitative measure of smoke-AOD from the AE difference at the IR-UV band.

In addition to the ground profilers, the NASA airborne HALO lidar made flight measurements on Aug.15-16 in the NYC area. Fig. 9 shows the aerosol optical thickness (AOT), time-height distribution, and optical properties of aerosols along the flight tracks on Aug.16, 2018. Multiple aerosol layers can be observed below 5-km altitude as indicated by strong aerosol backscatters, and some low-level plumes mixed down into the PBL by showing enhanced backscatter coefficients that are consistent with the ground CCNY-lidar observations. Importantly, the aloft plumes indicate smaller particle depolarization ratio (PDR) at 1064-nm than those in the PBL (<1.5 km altitude); but the PDRs at 532-nm are similar for the aloft dense plumes at 2.0-4.0 km and the aerosols in the PBL with the value at 0.055-0.08. Such spectral differences of PDRs for the smoke aerosols are related to fine-mode dominant particle size, near-spherical shape, and their coatings (Mishchenko et al., 2016; Gialitaki et al., 2020). In addition, the lidar-ratios at 532-nm are higher for the aloft plumes than those in the PBL. According to the aerosol extinction profiles measured from the HALO, the aloft smoke above the PBL contribute 70~80% of the total AOD in the NYC area. To further explore the optical differences of aerosols at the different altitudes, their histograms at the near surface (<0.5 km), PBL or mixing zone (0.5-1.5 km) and aloft plume layer (2.5-4.7 km) are plotted in Fig. 10, respectively, as well as for the near-surface data before the plume intrusion in the morning of Aug.15. It can be seen that the PDRs at 1064-nm on Aug.16 have much lower values (<0.03) for the aloft smoke particles but show larger values (~ 0.06) for the near surface aerosols.

371 Logically, the overlap region between 0.5-1.5 km altitude indicates the mixture of smoke particles with
372 the urban aerosols in the PBL. Meanwhile, the histograms of lidar-ratios indicate the peak value at 70-sr
373 for the aloft plume but at 50-sr for the near surface aerosols. Again, the overlap histograms for the data at
374 0.5-1.5 km indicate the mixture of the smoke with local urban aerosols. From the histograms of the near-
375 surface aerosols ("surf" vs. "surf_bg" in the morning of Aug.15) in Fig.10 (a-b), the PDR and lidar-ratio
376 also indicate distinct differences before and after the smoke intrusion. The further information of aerosol
377 optical properties in the morning of Aug.15 (before the dense plume intrusion) is given in Fig. S1-S2 (see
378 the Supporting Document). Overall, the smoke particles show different optical properties from local
379 urban aerosols that can help classify them.

380 Critical to our study, the UMD Cessna aircraft also made vertical distribution measurements of
381 the aerosol and trace gases on Aug. 16 on the south-shore of Long Island. Fig.11 shows the flight tracks
382 and the vertical distribution of aerosol and gaseous compounds. Concurrent strong aerosol scattering and
383 CO concentration indicate two-layers of smoke-like plumes at 2.3-3.2 km and in the PBL. The strong
384 wavelength dependence of the Aethalometer reading (nominally BC) indicated brown carbon (BrC) in the
385 plume aloft (See Fig.S3 in the Supporting Document). Moreover, the O_3 and BC also show high values in
386 the elevated smoke layers. The single scattering albedos (SSA) of aerosols are generally in the range of
387 0.70-0.93 at 565-nm, and the smoke layers indicate the lower SSA of 0.80 ± 0.05. In addition, the NOx
388 (NO_2 + NO) measurement indicates local maxima at 2.5-3.5 km altitude whereas there are high loadings
389 of CH_4 and formaldehyde (HCHO) at 1.0-2.5 km altitude. In contrast, Fig.S4 (see the Supporting
390 Document) shows the vertical profiles of aerosol and gaseous compounds in the PBL at noon of Aug.15
391 near the NYC area, before the dense smoke intrusions in the PBL. Overall, the aircraft in-situ
392 measurements indicate high-loadings of CO, O_3, BC, BrC, CH_4 and HCHO in the elevated smoke layers
393 that were transported from the Pacific Northwest and Canada. We further make the inter-comparisons of
394 aerosol optical properties and their vertical distribution among the NASA-HALO, UMD aircraft and
395 CCNY-lidar, with the summary Fig.12 indicating their good agreement. The comparison of ozone profiles

between the NASA-LMOL and UMD aircraft measurement shows good consistence as shown in Fig.S5 (see the Supporting Document).

3.3 Impacts on the air quality in NYC

The ground-level $PM_{2.5}$ and its species of OC and BC in NYC area are shown in Fig.13. First, $PM_{2.5}$ increased significantly from 5 to 30 $\mu g/m^3$ on Aug. 15, and these high values were persistent through the episode on Aug. 16-17. The consistently high $PM_{2.5}$ in the NYC urban and upwind rural site at Newburgh indicate similar regional sources of aerosols associated with the smoke transport. Meanwhile, the OC showed similar increase trends (from 4 to 11 $\mu g/m^3$) along with the BC increase as shown in Fig.13 (b). The delta-C (BC_{UV}-BC_{IR} in Fig.13(c)) increased by three times on Aug.16-17 in comparison to the values on the other days. The hourly O_3 in Fig.13(d) shows higher values (reaching hourly averages > 70 ppb) on Aug.16-17 in NYC area, while the CO indicated dramatic enhancements (not shown here). We further investigate the connection between the increments of OC and $PM_{2.5}$, CO and $PM_{2.5}$, respectively. As shown in Fig.14, they indicate strong correlation with the linear correlation coefficient R=0.9~0.95. These concurrent high-loadings of OC, CO, BC and delta-C indicate the strength and overall consistency of wildfire smoke-associated impacts.

3.4 Evaluation of NAQFC model forecast

Using these comprehensive measurements, we made a comparison to the NOAA NAQFC predictions of $PM_{2.5}$, O_3 and PBLH, as well as their vertical distributions of $PM_{2.5}$ and O_3. Initially, the ground O_3 and PBLH show similar diurnal variation between the model and observation, but the model showed systematic underestimates of O_3 during the daytime (Fig.15(b)). The ground $PM_{2.5}$ showed consistency between the predictions and observations on Aug.15, but was overestimated by the model in the mornings of Aug.16 and 17 in Fig.15 (a). The PBLHs agreed well in terms of their diurnal variation whereas the overestimate by the model can be seen in the early morning in Fig.15(c), which may affect the vertical mixing of $PM_{2.5}$ and O_3 near the surface. We note the different definitions for the PBLH between the

model and lidar observation. The model PBLH is based on Richardson number threshold while the lidar-ceilometer measured PBLH is estimated from the vertical gradient of aerosol distribution, this may also bring bias for their comparison. Further, we compare the vertical distribution of aerosol and O_3 between the model and lidar observations. As shown in Fig.16, the model product generally missed the dense smoke layer below 4-km altitude but captured the thin plumes above 4-km (Fig.16 a-b). Furthermore, the observed high-level ozone in the aloft smoke layer (Fig.6b) were also missed by the model as shown in Fig.16(c) since the current NAQFC does not include gas-phase emissions from wildfire smoke. Such large bias for the smoke plume aloft in the current model product is probably related to the smoke emission, injection height and intensity in the wildfire source region, meteorology-relevant transport and complex chemical process, which need further analysis and investigation.

3.5 Discussions

Differentiating aged smoke particles from local urban aerosols is important to quantify the smoke impacts on air quality and to evaluate modeling results. Chemical composition often provides direct elemental measurement of aerosol compounds but the method requires air sampling and/or traditional lab analysis techniques. Thus, the need to supplement with the optical remote sensing methods is critical for a comprehensive interpretation. In this study, we show the dramatic differences of aerosol depolarization ratio at 1064-nm and lidar-ratio at 532-nm between the smoke particles and urban aerosols from the NASA-HALO measurements. Meanwhile, the mixture of smoke with urban aerosols can be indicated from the variations of optical parameters at different altitudes. Previous numerical simulations with T-Matrix method by Mishchenko (2016) and Gialitaki (2020) indicate that the spectral differences of smoke aerosol depolarization ratios at 532-1064 nm mainly depend on the particle size and near-spherical shape with an axial ratio (a/b=0.9-1.2). The smoke particle depolarization ratios at 1064-nm are generally smaller than those at 532-nm. On the other hand, the smoke aerosols show larger lidar-ratio than urban aerosols due to stronger absorption and smaller backscatter coefficient associated with the size variation of aerosols, which are consistent with other observations (Burton et al., 2013, 2015).

In addition, the Angstrom exponent (AE) at the IR and UV bands show different variation trend along the dense smoke intrusions, their absolute differences show strong correlation with the smoke-AOD at both CCNY and BNL sites. Such correlation indicates that the smoke fraction in the total AOD can be potentially derived from the difference of AEs at IR and UV band. With the aerosol size distribution and refractive index retrieved by AERONET, we further analyzed the variation of AE at IR-UV using the Mie-scattering simulation (not shown here), and the results are consistent with the directly-measured AE spectral dependence in Fig.7-8. In addition, Eck et al. (1999) found that for the biomass burning aerosols, the AE show smaller values at 380-440 nm than those at 675-870 nm. A good correlation between the AE and fine-mode fraction of aerosols have been reported (O'Neill et al., 2003, Anderson et al., 2005).

Unfortunately, it is still difficult to quantify the smoke transport contribution to the total $PM_{2.5}$ at the ground level due to their mixture with local aerosols. Some biomarkers can be used to identify the smoke particles, such as delta-C and potassium iron, PAHs etc. (Dreessen et al., 2016, Wang et al., 2012). In this study, we observed that the delta-C values increased by three times compared to that of non-smoke days. In addition, the high correlation of $PM_{2.5}$ in the NYC urban and upwind rural area indicates the transport and regional scope of these smoke effects. Other measurements can also provide suitable diagnostic markers such as the strong correlations between the CO and smoke scattering coefficients, and the increments of OC and $PM_{2.5}$. These dramatic enhancements of carbonaceous aerosols are strongly associated with the transported wildfire smoke. In addition, we also see the enhancements of CO, BC, NOx, CH_4, and HCHO in the elevated smoke layers, which can produce increased O_3 through photochemical processes. We also observed that the vertical and horizontal transport or dispersion from the aloft O_3 layers affect the surface O_3. Dramatic enhancements of O_3 in the PBL were observed along the dense smoke intrusion on Aug.16 in comparison to the data on Aug.15. From a local pollution perspective, even with the long-range transport from the Pacific Northwest to the northeast US, there are still high levels of BC observed in the aloft smoke layer. In addition, Huang et al (2020) and Rogers et al (2020) indicated the increase of surface-level $PM_{2.5}$ for this event in the upstate of NYS and NYC-

Connecticut coastal region. The synoptic subsidence, strong PBL entrainment and vertical mixing resulted in the aloft smoke mixing into PBL on Aug.16 (Huang et al., 2020).

Finally, our comparisons between the model product and observations indicate consistency of the diurnal variation of PBL-height and O_3 with some exceptions. These include the overestimate of $PM_{2.5}$ by the model in the morning and night. The high O_3 concentrations clearly appeared in the elevated smoke layer from both ground lidar (Fig. 16) and aircraft measurements (Fig. 11). Such high O_3 can be vertically dispersed and transported to the near ground during the period of convective PBL. On the other hand, the systematic underestimate of O_3 by the model during the daytime may be more indicative of underestimates of chemical precursors of O_3 from the smoke transport (Dreessen et al., 2016). For the ground $PM_{2.5}$, the dramatic bias occurs in the early morning and night (i.e. weak convective PBL period) when the vertical mixing may play a major role. This might be improved by considering the urban canopy, urban Building Energy Model and Parameterization (BEM/BEP) that drive vertical mixing and transport near the surface (Gutiérrez and González, 2015).

4. Conclusions

In this work, we presented synergistic remote sensing and in-situ observations to study the transported dense wildfire smoke and its impact on air quality in the New York City and Long Island Sound areas during the LISTOS 2018 summer campaign. The time-height distribution, optical properties and gaseous compounds of smoke plumes were investigated from the aircraft, ground-based lidars and in-situ sensors on August 15-17, 2018. Vertical profiles of aerosol and O_3 along with the winds indicate that the smoke plumes affected the air quality through PBL advection, vertical mixing and subsidence. The comparisons among the different observations and retrievals of aerosol and ozone profiles show consistency.

Concurrent high loadings of aerosols, CO, O_3, BC, BrC, and NOx were observed in the elevated smoke layers transported from the Pacific Northwest. In particular, O_3 concentrations were above 70-ppb (NAAQS value) in the plume layers while CO and aerosol extinctions showed a strong correlation; CH_4 and HCHO also showed enhancements in the PBL.

The smoke aerosols showed different spectral behavior of particle depolarization ratio at 1064 nm and lidar-ratio at 532-nm from the urban aerosols. The observations from the Aethalometer showed a strong wavelength dependence in the elevated smoke plume, but not in the PBL indicating the dominance of BrC in the plume encountered between 2.5 and 3.0 km altitude and the dominance of BC between the surface and 1.5 km. Smoke particles can be discriminated from the urban aerosols by showing lower depolarization ratio (0.02) at 1064-nm and larger lidar-ratio (~70 sr at 532 nm). Their histogram distributions at different altitudes indicate the mixture of smoke with the local urban aerosols in the PBL and near surface. In addition, the extinction-related Angstrom Exponents at IR (1020-1640 nm) and UV (340-440nm) from AERONET observations show reverse variation trend along the smoke loadings, and their absolute differences indicate strong correlation with the smoke-AOD.

With the wildfire smoke intrusions, the ground-level $PM_{2.5}$, OC and CO show consistent and quick increase on August 15-17, 2018. The near-surface $PM_{2.5}$ increases from 5 to 30 $\mu g/m^3$ with the dominant contribution from the organic matter (~45%) in the NYC area. The increments of OC, CO, and $PM_{2.5}$ show strongly linear correlation with R greater than 0.9. As a biomarker of wood combustion, the delta-C increase by a factor of three. The $PM_{2.5}$ in NYC urban area show a good linear correlation (R=0.9) with those in the upwind rural area, indicating the impact of regional transport.

Compared to the observations, the NOAA NAQFC modeling forecast product shows consistent PBLH and $PM_{2.5}$ in the convective period of PBL, but lower O_3 at ground level, which is reasonable since the current NAQFC does not include gas-phase emissions from wildfire smoke. The large biases for the modeled PBLH and ground $PM_{2.5}$ mainly occurred in the morning and night when vertical mixing and convection were weak.

Acknowledgements. This study is in part supported by the New York State Energy Research Development Authority (NYSERDA) (grant # 101132 and 137482), Northeast States for Coordinated Air Use Management (NESCAUM) (grant # 2411 and 2417) and the National Oceanic and Atmospheric Administration- Cooperative Science Center for Earth System Sciences and Remote Sensing

Technologies (NOAA-CESSRST) under the Cooperative Agreement Grant # NA16SEC4810008. The funding agencies have not reviewed the paper, and it does not necessarily reflect the views or policies of NYSERDA, NESCAUM, NYSDEC, or NOAA. Authors greatly appreciate the data from NASA-AERONET, NOAA-HMS, HYSPLIT and NAQFC model, NYSDEC and NYS-Mesonet operated by SUNY-Albany. In particular, we appreciate Oliver Rattigan of NYSDEC for providing OC and BC data. The NASA airborne measurements during LISTOS would not have been possible without the support of the NASA GEO-CAPE Mission Study as well as NASA ESD Tropospheric Composition Program to enable ground-based ozone lidar and the HALO airborne lidar to participate in the LISTOS campaign. UMD flights were supported by NESCAUM, National Fish and Wildlife Foundation, NIST, NOAA/ARL, and MDE. This research is made possible by the New York State (NYS) Mesonet. Original funding for the NYS Mesonet was provided by Federal Emergency Management Agency grant FEMA-4085-DR-NY, with the continued support of the NYS Division of Homeland Security & Emergency Services; the state of New York; the Research Foundation for the State University of New York (SUNY); the University at Albany, SUNY; the Atmospheric Sciences Research Center (ASRC) at SUNY Albany; and the Department of Atmospheric and Environmental Sciences (DAES) at SUNY Albany. We gratefully acknowledge the valuable comments from two anonymous reviewers.

References

Anderson, T. L., Wu, Y., Chu, D. A., Schmid, B., Redemann, J., Dubovik, O., 2005. Testing the MODIS satellite retrieval of aerosol fine-mode fraction, J. Geophys. Res., 110, D18204.

Andreae, M. O., Browell, E. V., Garstang, M., Gregory, G. L., Harriss, R. C., Hill, G. F., Jacob, D. J., Pereira, M. C., Sachse, G. W., Setzer, A. W., Dias, P. L. S., Talbot, R. W., Torres, A. L., and Wofsy, S. C.: Biomass-burning emissions and associated haze layers over Amazonia, J. Geophys. Res., 93, 1509, 1988.

Ansmann, A., Baars, H., Chudnovsky, A., Mattis, I., Veselovskii, I., Haarig, M., Seifert, P., Engelmann, R., and Wandinger, U., 2018: Extreme levels of Canadian wildfire smoke in the stratosphere over central Europe on 21–22 August 2017, Atmos. Chem. Phys., 18, 11831–11845.

Brooks, I., 2003. Finding boundary layer top: Application of a wavelet covariance transform to lidar backscatter profiles, J. Atmos. Oceanic Technol., 20, 1092-1105.

Brotzge, J. A., and Coauthors, 2020: A Technical Overview of the New York State Mesonet Standard Network. J. Atmos. Oceanic Technol., 37, 1827–1845, https://doi.org/10.1175/JTECH-D-19-0220

551 Burton, S. P., R. A. Ferrare, M. A. Vaughan, A. H. Omar, R. R. Rogers, C. A. Hostetler, J. W. Hair, 2013.
552 Aerosol classification from airborne HSRL and comparisons with the CALIPSO vertical feature
553 mask, Atmos. Meas. Tech., 6, 1397–1412.
554 Burton, S. P., Vaughan, M. A., Ferrare, R. A., and Hostetler, C. A., 2014. Separating mixtures of aerosol
555 types in airborne High Spectral Resolution Lidar data, Atmos. Meas. Tech., 7, 419–436.
556 Burton, S. P., Hair, J. W., Kahnert, M., Ferrare, R. A., Hostetler, C. A., Cook, A. L., Harper, D. B.,
557 Berkoff, T. A., Seaman, S. T., Collins, J. E., Fenn, M. A., and Rogers, R. R., 2015. Observations of
558 the spectral dependence of linear particle depolarization ratio of aerosols using NASA Langley
559 airborne High Spectral Resolution Lidar, Atmos. Chem. Phys., 15, 13453-13473.
560 Castellanos, P., L. T. Marufu, B. G. Doddridge, B. F. Taubman, S. H. Ehrman, R. R. Dickerson, 2011,
561 Ozone, nitrogen oxides, and carbon monoxide during pollution events over the eastern US: An
562 evaluation of emissions and vertical mixing, J. Geophys. Res., 116, D16307.
563 Chillrud, S., Dobovicnik, T., Wu, Y., Yang, Q, Moshary, F., Arend, M., Blair, J., Markowitz, M.,
564 McGillis, W., Yan, B., 2019. Multi-wavelength microaeth data provide specific tracers of ground
565 level air pollution impacts of long-range transport wildfire plumes in NYC in November 2018. Air
566 Quality and Climate Change, 53(4), 32-33.
567 Colarco, P. R., Schoeberl, M. R., Doddridge, et al. 2004. Transport of smoke from Canadian forest fire to
568 the surface near Washington, D.C.: Injection height, entrainment, and optical properties. J. Geophy.
569 Res., 109, D06203.
570 Crawford, J., Dickerson, R., Hains, J., DISCOVER-AQ: Observations and Early Results, Environ.
571 Manag., 2014, https://www.awma.org/emsept14.
572 Crutzen, P. J., Heidt, L. E., Krasnec, J. P. 1979. Biomass Burning As a Source of Atmospheric Gases
573 CO, H_2, N_2O, NO, CH_3Cl, and COS, Nature 282(5736), 253–356.
574 Dennison, P. E., S. C. Brewer, J. D. Arnold, and M. A. Moritz, 2014. Large wildfire trends in the western
575 United States, 1984–2011. Geophys. Res. Lett., 41, 2928–2933.
576 Draxler, R.R., Hess, G.D., 1997. Description of the HYSPLIT_4 modeling system. NOAA Tech. Memo.
577 ERL ARL-224, NOAA Air Resources Laboratory, Silver Spring, MD, 24.
578 Dreessen, J., Sullivan, J., Delgado, R., 2016. Observations and impacts of transported Canadian wildfire
579 smoke on ozone and aerosol air quality in the Maryland region on June 9–12, 2015, J. Air & Waste
580 Management Assoc., 66:9, 842-862.
581 Eck, T. F., B. N. Holben, J. S. Reid, et al., 1999. Wavelength dependence of the optical depth of biomass
582 burning, urban, and desert dust aerosols, J. Geophys. Res., 104, 31,333–31,349.
583 Farris, B. M., Gronoff, G. P., Carrion, W., Knepp, T., Pippin, M., and Berkoff, T. A., 2019.
584 Demonstration of an off-axis parabolic receiver for near-range retrieval of lidar ozone profiles,
585 Atmos. Meas. Tech., 12, 363–370.
586 Foley, K. M., Roselle, S. J., Appel, K. W., Bhave, P. V., Pleim, J. E., Otte, T. L., Mathur, R., Sarwar, G.,
587 Young, J. O., Gilliam, R. C., Nolte, C. G., Kelly, J. T., Gilliland, A. B., and Bash, J. O., 2010.
588 Incremental testing of the Community Multiscale Air Quality (CMAQ) modeling system version 4.7,
589 Geosci. Model Dev., 3, 205-226.

590 Gan, C., Wu, Y., Madhavan, B., Gross, B., Moshary, F., 2011. Application of active optical sensors to
591 probe the vertical structure of the urban boundary layer and assess anomalies in air quality model
592 PM2.5 forecasts, Atmos. Environ., 45 (37), 6613-6621.
593 Gialitaki, A., Tsekeri, A., Amiridis, V., Ceolato, R., Paulien, L., Proestakis, E., Marinou, E., Haarig, M.,
594 Baars, H., Balis, D., 2020. Is near-spherical shape "the new black" for smoke? EPJ Web Conf. 237,
595 02017, DOI: 10.1051/epjconf/202023702017
596 Gronoff, G., J. Robinson, T. Berkoff, R. Swap, B. Farris, J. Schroeder, H. Halliday, T. Knepp, E. Spinei,
597 W. Carrion, E. Adcock, Z. Johns, D. Allen, M. Pippin, 2019. A method for quantifying near range
598 point source induced O_3 titration events using Co-located Lidar and Pandora measurements. Atmos.
599 Environ., 204, 43-52.
600 Gutiérrez, E., J.E. González, A. Martilli, R. Bornstein, M. Arend, 2015. Simulations of a Heat-Wave
601 Event in New York City Using a Multilayer Urban Parameterization. J. Appl. Meteor. Clima, 54,
602 283–301.
603 Haarig, M., Ansmann, A., Baars, H., Jimenez, C., Veselovskii, I., Engelmann, R., Althausen, D., 2018:
604 Depolarization and lidar ratios at 355, 532, and 1064 nm and microphysical properties of aged
605 tropospheric and stratospheric Canadian wildfire smoke, Atmos. Chem. Phys., 18, 11847–11861.
606 Haeffelin, M., Angelini, F., Morille, Y., Martucci, G., Frey, S., Gobbi, G.P., Lolli, S., O'Dowd, C.D.,
607 Sauvage, L., Xueref-Remy, I., Wastine, B., Feist, D.G., 2012. Evaluation of mixing-height retrievals
608 from automated profiling lidars and ceilometers in view of future integrated networks in Europe.
609 Boundary-Layer Meteorol. 143, 49–75.
610 Hair, J. W., C. A. Hostetler, A. L. Cook, D. B. Harper, R. A. Ferrare, T. L. Mack, W. Welch, L. R.,
611 Izquierdo, F. E. Hovis, 2008: Airborne High Spectral Resolution Lidar for Profiling Aerosol Optical
612 Properties, Appl. Opt., 47 (36), 6734-6752.
613 Han, Y., Wu, Y., Wang. T., Zhuang, B., Li S., Zhao K., 2015. Impacts of elevated-aerosol-layer and
614 aerosol type on the correlation of AOD and particulate matter with ground-based and satellite
615 measurements in Nanjing, southeast China, Science of The Total Environment, 532, 195-207.
616 Hoff, R. M., Christopher, S. A., 2009. Remote sensing of Particulate Pollution from Space: Have we
617 reached the Promised Land, J. Air Waste Manage. Assoc., 59, 645–675.
618 Holben, B.N., T. F. Eck, I. Slutsker, D. Tanré, J.P. Buis, A. Setzer, E. Vermote, J.A. Reagan, Y.J.
619 Kaufman, T. Nakajima, F. Lavenu, I. Jankowiak, A. Smirnov, 1998. AERONET - A federated
620 instrument network and data archive for aerosol characterization, Rem. Sens. Environ., 66, 1-16.
621 Huang, J., J. McQueen, J. Wilczak, I. Djalalova, I. Stajner, P. Shafran, D. Allured, P. Lee, L. Pan, D.
622 Tong, H. Huang, G. DiMego, S. Upadhayay, L. Monache, 2017. Improving NOAA NAQFC $PM_{2.5}$
623 predictions with a bias correction approach, Wea. and Forecasting, 32, 407-421.
624 Hung, W.T., Lu, C.H., Shrestha, B., Lin, H. C., Lin, C.A., Grogan, D., Hong, J., Ahmadov, R., James, E.,
625 Joseph, E., 2020. The impacts of transported wildfire smoke aerosols on surface air quality in New
626 York State: A case study in summer 2018, Atmos. Environ., 227, 117415.
627 Jaffe, D.A., Hafner, W., Chand, D., Westerling, A., Spracklen, D., 2008. Interannual Variations in PM2.5
628 due to Wildfires in the Western United States, Environ. Sci. Technol. 42 (8), 2812-2818.

Jaffe, D. A., Nicole L. W., 2012. Ozone production from wildfires: A critical review, Atmos. Environ., 51, 1-10.

Jaffe, D.A., Wigder N, Downey N, Pfister G, Boynard A, Reid SB, 2013. Impact of wildfires on ozone exceptional events in the Western U.S., Environ Sci Technol., 47(19):11065-72

Janjie, Z. I., J. P. Gerrity Jr., and S. Nickovic, 2001. An alternative approach to nonhydrostatic modeling. Mon. Wea. Rev., 129, 1164–1178.

Karambelas, A., LISTOS: Toward a Better Understanding of New York City's Ozone Pollution Problem (An overview of the Long Island Sound Tropospheric Ozone Study). The Magazine for Environmental Managers, A&WMA, October 2020, https://pubs.awma.org/flip/EM-Oct-2020/karambelas.pdf

Kelly, J. T., P. V. Bhave, C. G. Nolte, U. Shankar, K. M. Foley, 2009. Simulating emission and chemical evolution of coarse sea-salt particles in the Community Multiscale Air Quality (CMAQ) model. Geosci. Model Dev., 2, 1335–1374.

Kochanski, A. K., Mallia, D. V., Fearon,M. G., Mandel, J., Souri, A. H., Brown, T. 2019. Modeling wildfire smoke feedback mechanisms using a coupled fire-atmosphere model with a radiatively active aerosol scheme, J.Geophy. Res. Atmos., 124, 9099–9116.

Lall, R., Thurston, G. D., 2006. Identifying and quantifying transported vs. local sources of New York City PM2.5 fine particulate matter air pollution, Atmos. Environ., 40(2), 333-346.

Leblanc, T., Brewer, M. A., Wang, P. S., Granados-Muñoz, M. J., Strawbridge, K. B., Travis, M., Firanski, B., Sullivan, J. T., McGee, T. J., Sumnicht, G. K., Twigg, L. W., Berkoff, T. A., Carrion, W., Gronoff, G., Aknan, A., Chen, G., Alvarez, R. J., Langford, A. O., Senff, C. J., Kirgis, G., Johnson, M. S., Kuang, S., and Newchurch, M. J., 2018: Validation of the TOLNet lidars: the Southern California Ozone Observation Project (SCOOP), Atmos. Meas. Tech., 11, 6137–6162.

Lee, P., J. McQueen, I. Stajner, J. Huang, L. Pan, D. Tong, H. Kim, Y. Tang, Kondragunta S., M. Ruminski, S. Lu, E. Rogers, R. Saylor, P. Shafran, H. Huang, J. Gorline, S. Upadhayay, R. Artz, 2017. NAQFC developmental forecast guidance for fine particulate matter (PM2.5). Wea. and Forecasting. 32 (1): 343–360.

Li, S., Joseph, E., Min, Q., 2016. Remote sensing of ground-level PM2.5 combining AOD and backscattering profile, Remote Sensing of Environment, 183, 120-128.

Li, Z. Q., Guo, J. P., Ding, A. J., Liao, H., Liu, J. J., Sun, Y. L., et al. 2017. Aerosol and boundary-layer interactions and impact on air quality. National Science Review, 4(6), 810–833.

Lin, C., Li, Y., Yuan, Z., Lau, K.H., Li, C., Fung, C.H., 2015. Using satellite remote sensing data to estimate the high-resolution distribution of ground-level PM2.5, Remote Sensing of Environment, 156, 117-128.

Liu, Y., Wang, Z., Wang, J., Ferrare, R. A., Newsom, R. K., Welton, E. J., 2011. The effect of aerosol vertical profiles on satellite-estimated surface particle sulfate concentrations, Remote Sensing of Environment, 115 (2), 508-513.

Liu, Y., Goodrick, S., Heilman, W., 2014. Wildland fire emissions, carbon, and climate: Wildfire–climate interactions. Forest Ecol. Manage., 317, 80–96

McKendry, I. G., Christen, A., Lee, S.-C., Ferrara, M., Strawbridge, K. B., O'Neill, N., Black, A. 2019. Impacts of an intense wildfire smoke episode on surface radiation, energy and carbon fluxes in southwestern British Columbia, Canada, Atmos. Chem. Phys., 19, 835–846.

Menut, L., Flamant, C., Pelon, J., Flamant, P.H., 1999. Urban boundary-layer height determination from lidar measurements over the Paris area. Appl. Opt. 38, 945–954.

Mishchenko, M. I, J. M. Dlugach, L. Liu, 2016. Linear depolarization of lidar returns by aged smoke particles, Appl. Opt. 55, 9968-9973.

Miller, P. J., 2017. Retrospective and Future Analysis of Air Quality In and Downwind of New York City, DRAFT White Paper, available at www.nescaum.org/documents/listos.

Mok, J., Krotkov, N. A., Arola, A., Torres, O., Jethva, H., Andrade, M., Labow, G., Eck, T. F., Li, Z., Dickerson, R. R., Stenchikov, G. L., Osipov, S., & Ren, X. 2016. Impacts of brown carbon from biomass burning on surface UV and ozone photochemistry in the Amazon Basin. Scientific Reports, 6, 36940.

National Research Council (2009), Global Sources of Local Pollution: An Assessment of Long-Range Transport of Key Air Pollutants to and From the United States, The National Academies Press, Washington, D. C.

Nehrir, Amin R., Kiemle, Christoph, Lebsock, Mathew D. Kirchengast, Gottfried, Buehler, Stefan A. Löhnert, Ulrich, Liu, Cong-Liang, Hargrave, Peter C., Barrera-Verdejo, Maria, Winker, David M., 2017. Emerging Technologies and Synergies for Airborne and Space-Based Measurements of Water Vapor Profiles, Surveys in Geophysics, 38 (6), 1445–1482.

Nehrir, A. Notari, A., Harper, D., Fitzpatrick, F., Collins, J., Kooi, S., Antill, C., Hare, R., Barton-Grimley, R., Hair,J., Ferrare,R., Hostetler, C., Welch,W., The High Altitude Lidar Observatory (HALO): A multi-function lidarand technology test-bed for airborne and space-based measurements of water vapor and methane, The NASA Earth Science Technology Forum (ESTF2018), June 12-14, 2018 in Silver Spring, MD, https://esto.nasa.gov/forum/ESTF2018/abstracts/nehrir.htm

O'Neill, S. M., and Coauthors, 2009. Regional real-time smoke prediction systems. Wildland Fires and Air Pollution, A. Bytnerowicz et al., Eds., Developments in Environmental Science, 8, Elsevier, 499–534.

O'Neill, N. T., T. F., Eck, A. Smirnov, B. N.Holben, S. Thulasiraman, 2003. Discrimination of coarse and fine mode optical depth, J. Geophys. Res., 108 (D17), 4559-4573.

Pachon, J. E., Weber, R. J., Zhang, X., Mulholland, J. A., Russell, G.A. 2013. Revising the use of potassium (K) in the source apportionment of $PM_{2.5}$, Atmos. Pollution Res., 4(1), 14-21.

Rattigan, O. V., H. D. Felton, M.S. Bae, J. J. Schwab, K. L. Demerjian, 2010. Multi-year hourly PM2.5 carbon measurements in New York: Diurnal, day of week and seasonal patterns, Atmos. Environ., 44 (16), 2043-2053.

Rattigan, O.V., Civerolo, K., Doraiswamy, P., Felton, H.D. and Hopke, P.K. 2013. Long Term Black Carbon Measurements at Two Urban Locations in New York. Aerosol Air Qual. Res. 13: 1181-1196.

Rattigan, O. V., K. L. Civerolo, H. D. Felton, J. J. Schwab, K. L. Demerjian, 2016. Long Term Trends in New York: $PM_{2.5}$ Mass and Particle Components, Aerosol Air Qual. Res, 16(5), 1191-1205.

Ren, X., O. E. Salmon, J. R. Hansford, D. Ahn, D. Hall, S. E. Benish, P. R. Stratton, H. He, S. Sahu, C. Grimes, A. M. F. Heimburger, C. R. Martin, M. D. Cohen, B. Stunder, R. J. Salawitch, S. H. Ehrman, P. B. Shepson, R. R. Dickerson, 2018. Methane Emissions from the Baltimore-Washington Area Based on Airborne Observations: Comparison to Emissions Inventories, J. Geophys. Res., 123, 8869–8882.

Ren, X., D. L. Hall, T. Vinciguerra, S. E. Benish, P. R. Stratton, D. Ahn, J. R. Hansford, M. D. Cohen, S. Sahu, H. He, C. Grimes, J. D. Fuentes, P. B. Shepson, R. J. Salawitch, S. H. Ehrman, and R. R. Dickerson, 2019. Methane emissions from the Marcellus Shale in southwestern Pennsylvania and northern West Virginia Based on Airborne Measurements, J. Geophys. Res. Atmos., 124, 1862–1878.

Rogers, H. M., Ditto, J. C., Gentner, D. R. 2020. Evidence for impacts on surface-level air quality in the northeastern US from long-distance transport of smoke from North American fires during the Long Island Sound Tropospheric Ozone Study (LISTOS) 2018, Atmos. Chem. Phys., 20, 671–682.

Ruminski, M., Kondragunta, S., Draxler, R., Zeng, J., 2006. Recent Changes to the Hazard Mapping System, 15th International Emission Inventory Conference, Reinventing Inventories - New Ideas in New Orleans, New Orleans, May 15 – 18, 2006.

Russell, P.B., R. W. Bergstrom, Y. Shinozuka, A. D. Clarke, P. F. DeCarlo, J. L. Jimenez, J. M. Livingston, J. Redemann, O. Dubovik, and A. Strawa. 2010. Absorption Angstrom Exponent in AERONET and related data as an indicator of aerosol composition, Atmos. Chem. Phys., 10, 1155-1169.

Sapkota, A., Symons, J. M., Kleissl, J., Wang, L., Parlange, M. B., Ondov, J., Breysse, P. N., Diette, G. B., Eggleston, P. A., Buckley, T. J. 2005. Impact of the 2002 Canadian Forest Fires on Particulate Matter Air Quality in Baltimore City, Environ. Sci. Technol., 39 (1), 24–32.

Scarino, A. J., Obland, M. D., Fast, J. D., Burton, S. P., Ferrare, R. A., Hostetler, C. A., Berg, L. K., Lefer, B., Haman, C., Hair, J. W., Rogers, R. R., Butler, C., Cook, A. L., and Harper, D. B.: Comparison of mixed layer heights from airborne high spectral resolution lidar, ground-based measurements, and the WRF-Chem model during CalNex and CARES, Atmos. Chem. Phys., 14, 5547–5560, https://doi.org/10.5194/acp-14-5547-2014, 2014

Schoennagel, T., J. K. Balch, H. Brenkert-Smith, P. E. Dennison, B. J. Harvey, M. A. Krawchuk, N. Mietkiewicz, P. Morgan, M. A. Moritz, R. Rasker, M. G. Turner, C. Whitlock, 2017. Adapt to more wildfire in western North American forests as climate changes, Proc. Natl. Acad. Sci., 114 (18), 4582-4590.

Schween, J.H., Hirsikko, A., Lohnert, U., Crewell, S., 2014. Mixing-layer height retrieval with ceilometer and Doppler lidar from case studies to long-term assessment. Atmos. Meas. Tech. 7, 3685–3704.

Stull, R.B., 1988. An Introduction to Boundary Layer Meteorology. Kluwer Academic Publishers, pp. 12–16.

Su, J., Liu, Z., Wu, Y., McCormick, P., Lei, L., 2013. Retrieval of multi-wavelength aerosol lidar ratio profiles using Raman scattering and Mie backscattering signals, Atmos. Environ., 79, 36-40.

Su, J., Wu, Y., McCormick, P., Lei, L., Lee R. 2014. Improved method to retrieve aerosol optical

properties from combined elastic backscatter and Raman lidar data, Appl. Phys. B, 116 (1), 61–67.

Tucker, S.C., Senff, C.J., Weickmann, A.M., Brewer, W.A., Banta, R.M., Berg, S.P., Law, D. C., Hardesty, R.M., 2009. Doppler idar estimation of mixing height using turbulence, shear, and aerosol profiles. J. Atmos. Ocean. Technol. 26, 673–688.

Taubman, B. F., L. T. Marufu, C. A. Piety, B. G. Doddridge, J. W. Stehr, R. R. Dickerson, 2004. Airborne characterization of the chemical, optical, and meteorological properties, and origins of a combined ozone-haze episode over the eastern United States, J. Atmos. Sci., 61, 1781-1793.

Vaughan, G., Draude, A. P., Ricketts, H. M. A., Schultz, D. M., Adam, M., Sugier, J., and Wareing, D. P., 2018: Transport of Canadian forest fire smoke over the UK as observed by lidar, Atmos. Chem. Phys., 18, 11375–11388.

Wang, Y., Hopke, P. K., Rattigan, O., Chalupa D., Utell, M., 2012. Multiple-year black carbon measurements and source apportionment using Delta-C in Rochester, New York, J. Air & Waste Manag. Assoc., 62:8, 880-887.

Wu, Y., Han, Y., Voulgarakis, A., Wang, T., Li, M., Wang, Y., Xie, M., Zhuang, B., and Li, S., 2017. An agricultural biomass burning episode in eastern China: Transport, optical properties, and impacts on regional air quality, J. Geophys. Res. (Atmos), 122, 2304– 2324.

Wu, Y., S. Chaw, B. Gross, F. Moshary, and S. Ahmed, 2009. Low and optically thin cloud measurements using a Raman-Mie lidar, Appl. Opt. 48, 1218-1227.

Wu, Y., L. Cordero, B. Gross, Moshary, F., Ahmed, S., 2012. Smoke plume optical properties and transport observed by a multi-wavelength lidar, sunphotometer and satellite, Atmos. Environ., 63, 32–42.

Wu, Y., Nazmi, C., Han, Z., Li, C., Gross, B., Moshary, F. 2016. Integrated Observation of Aerosol Plumes Transport and Impacts on the Air Quality Remote Sensing in the Northeast U.S., EPJ Web of Conferences 119, 18004, https://doi.org/10.1051/epjconf/201611918004

Wu, Y., A. Arapi, J. Huang, B. Gross, F. Moshary, 2018. Intra-continental wildfire smoke transport and impact on local air quality observed by ground-based and satellite remote sensing in New York City, Atmos. Environ., 187, 266-281.

Young, R. D., W. Carrion, R. Ganoe, D. Pliutau, G. Gronoff, T. Berkoff, S. Kuang, 2017. Langley mobile ozone lidar: ozone and aerosol atmospheric profiling for air quality research, Appl. Opt. 56, 721-730.

Zhang, Y., Li, Z., 2015. Remote sensing of atmospheric fine particulate matter (PM2.5) mass concentration near the ground from satellite observation, Remote Sensing of Environment,160, 252-262.

779

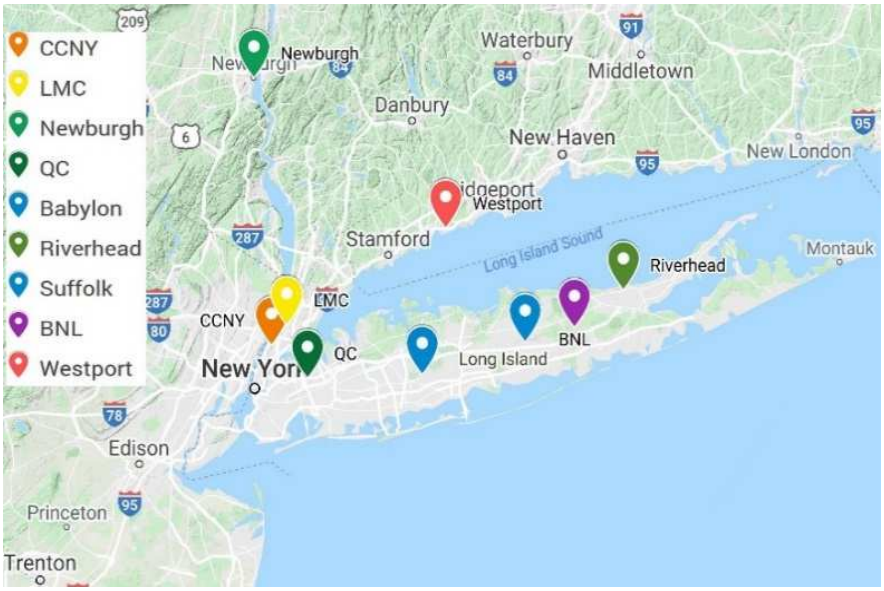

780

781 Fig.1 Ground-site map in the NYC and Long Island area (See the latitude and longitude in Table-1).

782

783

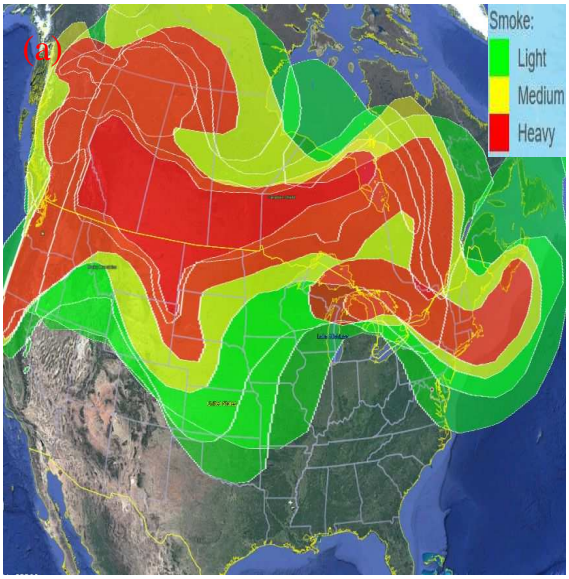

(b)

784

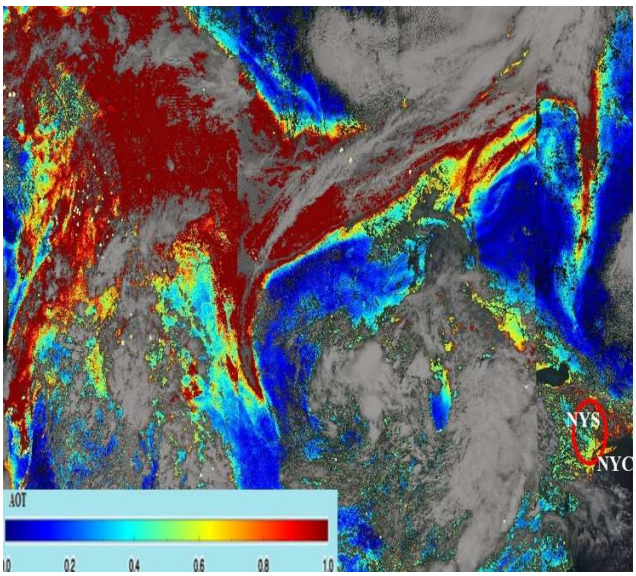

785

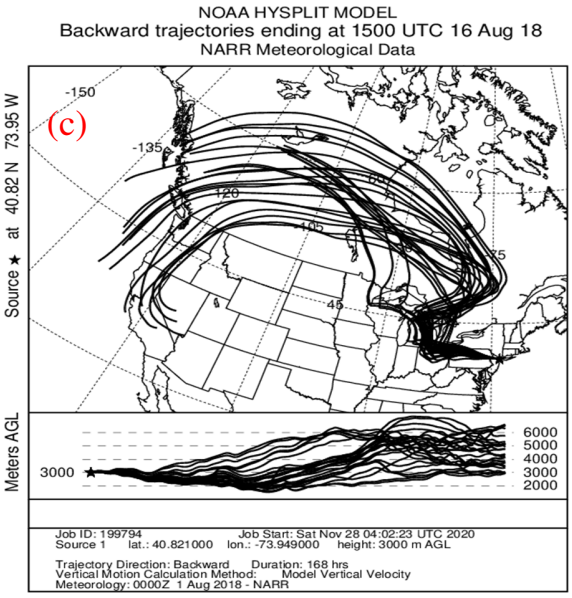

786

787 Fig.2 Wildfires smoke (color) from NOAA-HMS product (a), aerosol optical depth (AOD) at 550-nm
788 from the VIIRS satellite (red circle for NYS area) (b), and HYSPLIT ensemble backward trajectories (7-
789 day travel time) ending at 3-km altitude at CCNY at 15:00 UTC (c) on Aug.16, 2018.

790

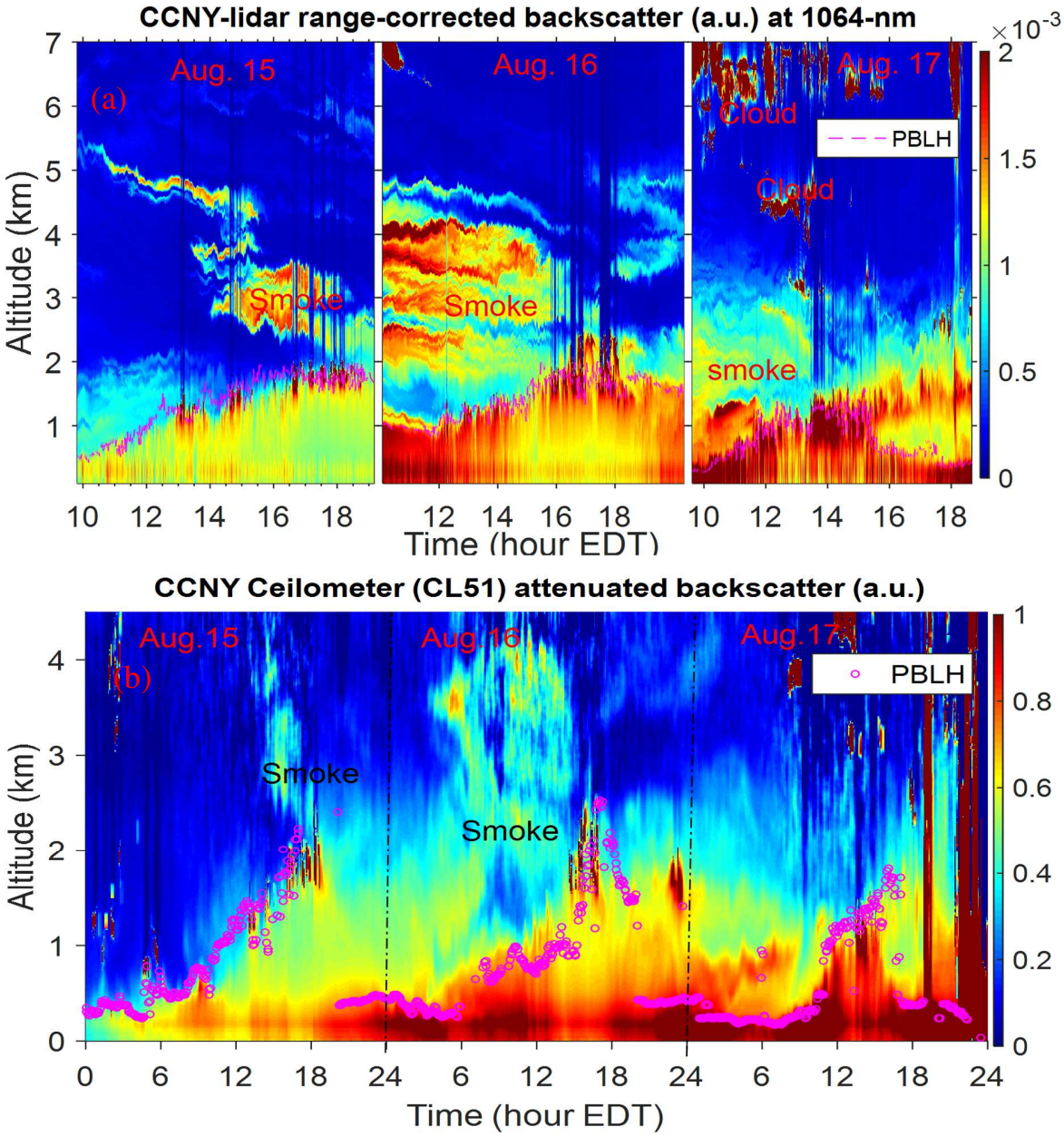

Fig.3 Time-height distribution of lidar (a) and ceilometer attenuated backscatter and PBLH (b) at CCNY on Aug.15-17, 2018

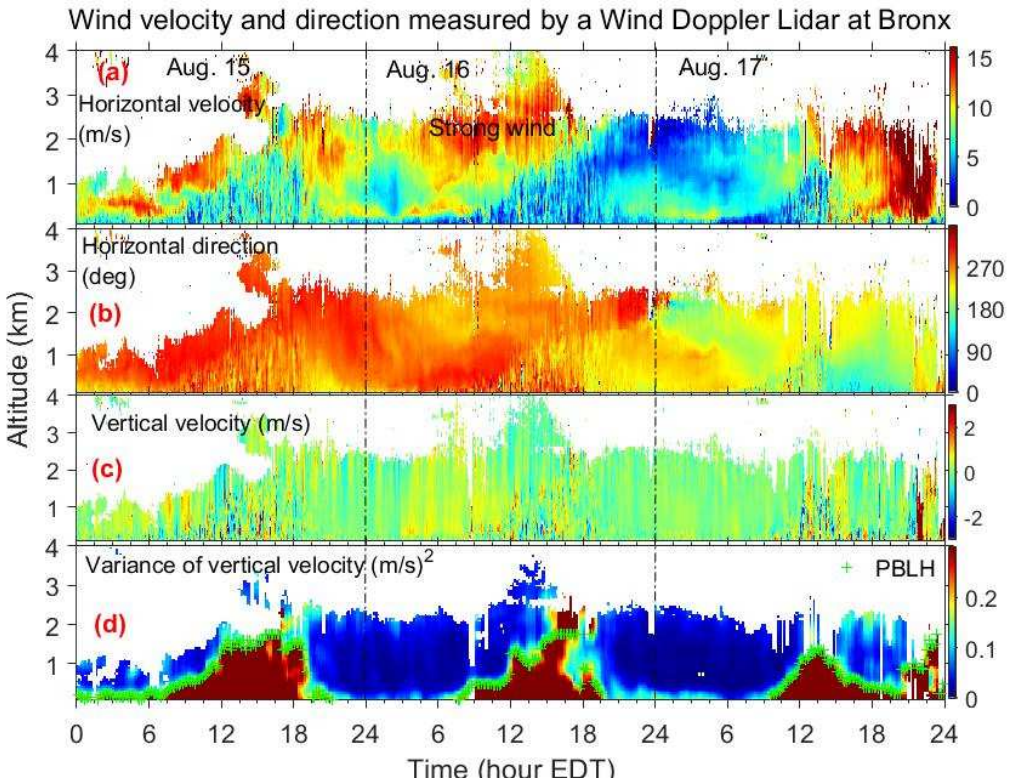

797

798 Fig.4 Horizontal wind velocity (a) and wind direction (b), vertical wind velocity (+ updraft, - downdraft)
799 (c), and variance of vertical wind velocity and inferred PBLH (d) from a Wind Doppler Lidar on Aug.15-
800 17, 2018. Strong horizontal winds at 1-3 km at 6:00-18:00 EDT on Aug.16 corresponding to the plume
801 layer; large variance of vertical velocity at 12:00-18:00 indicate strong turbulent mixing.

802

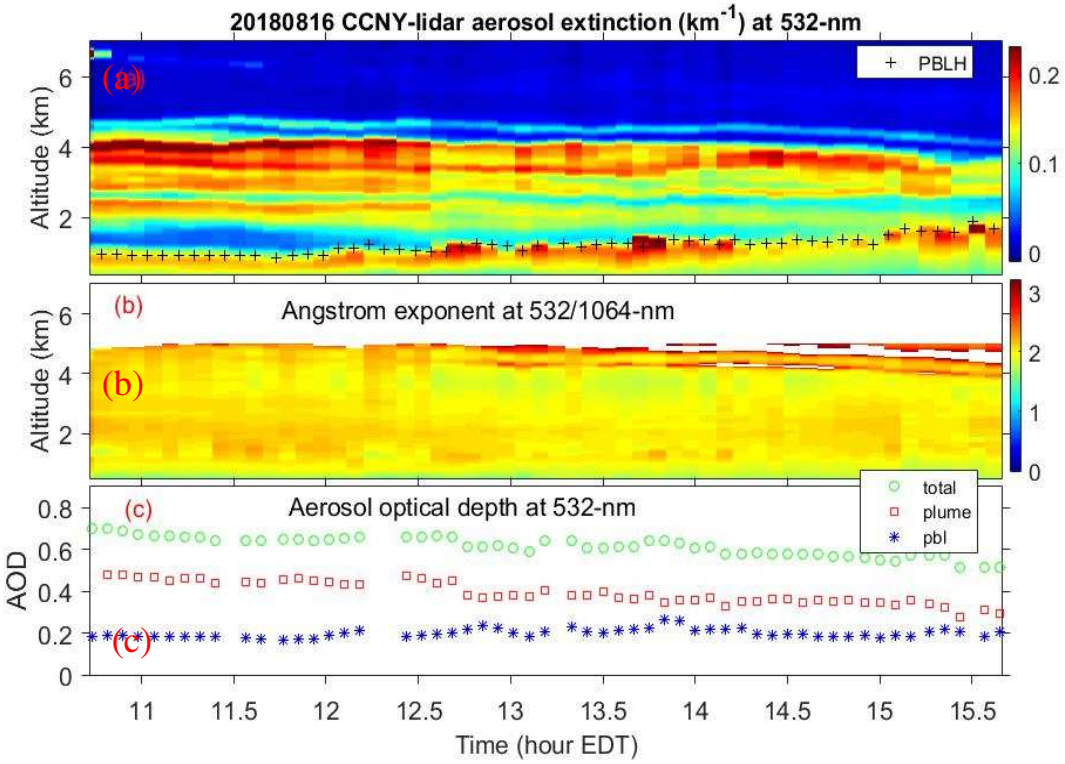

Fig.5 Aerosol extinction coefficient (a), Angstrom exponent (b) and aloft AOD (c) in 5-min average under the clear sky on Aug.16, 2018

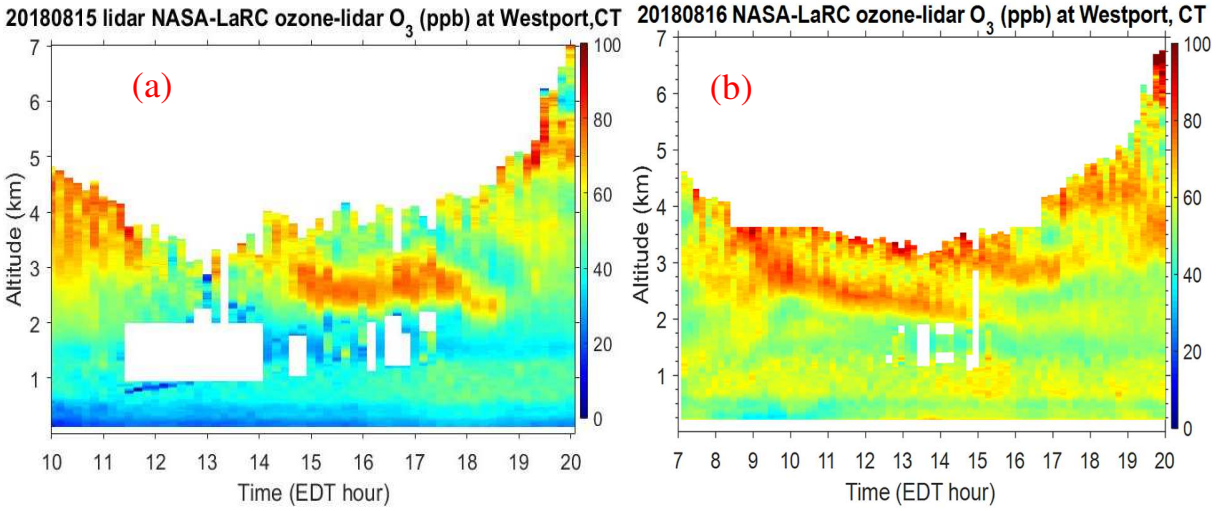

Fig.6 Vertical distribution of ozone concentrations measured by NASA LaRC ozone lidar on Aug.15 (a) and Aug.16 (b), 2018 in Westport, CT. (No retrieval made in the clouds and above 4.5 km altitude in the daytime due to the low SNR)

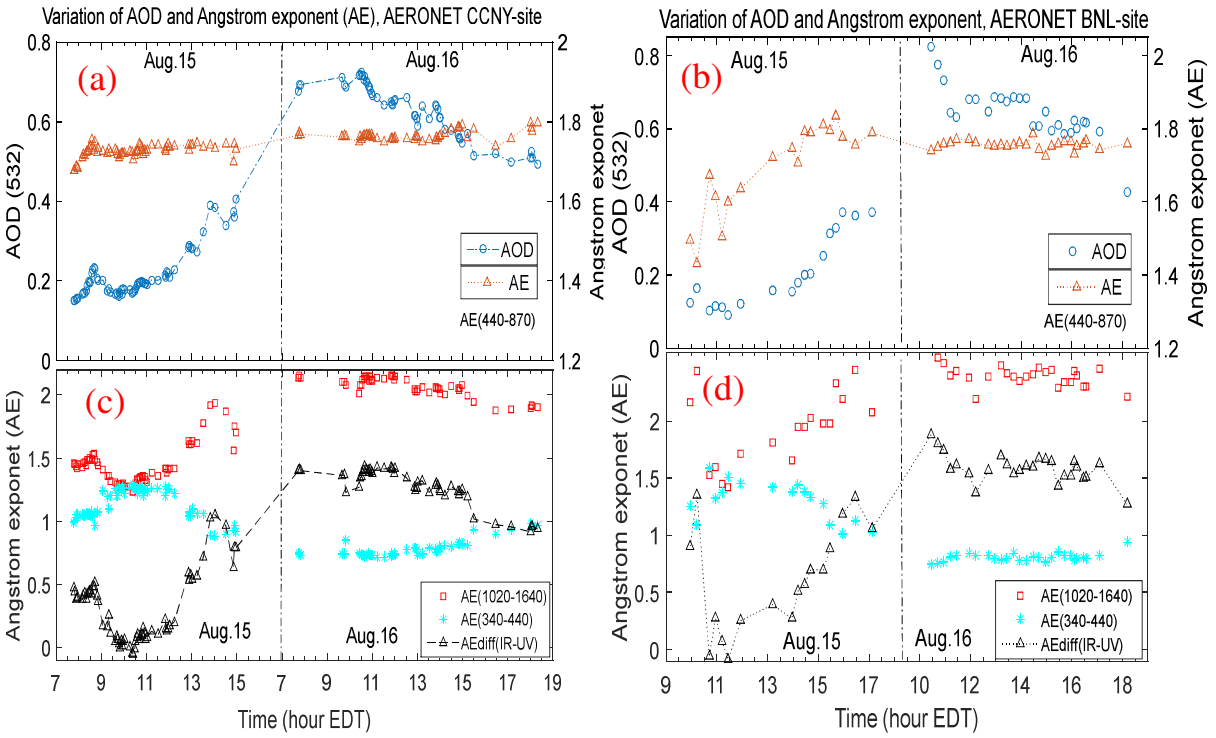

Fig.7 Aerosol optical depth (AOD) and Angstrom exponent (AE) measured by AERONET at the CCNY ((a) and (c)) and BNL ((b) and (d)) sites on Aug. 15-16, 2018

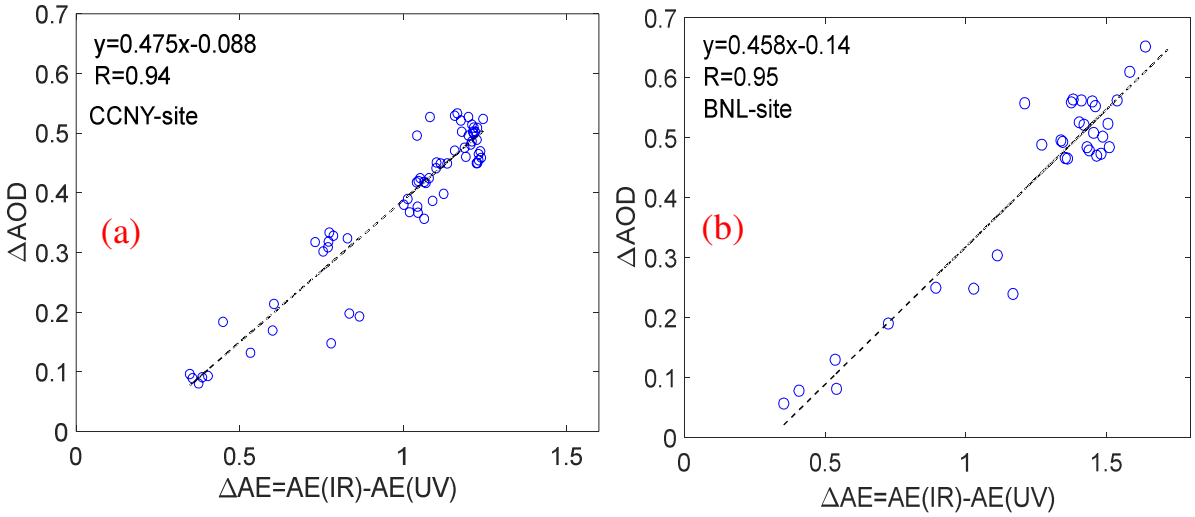

Fig.8 Correlation of Angstrom exponent difference (ΔAE) and smoke-AOD (ΔAOD) at the CCNY (a) and BNL (b) sites on Aug. 15-16, 2018

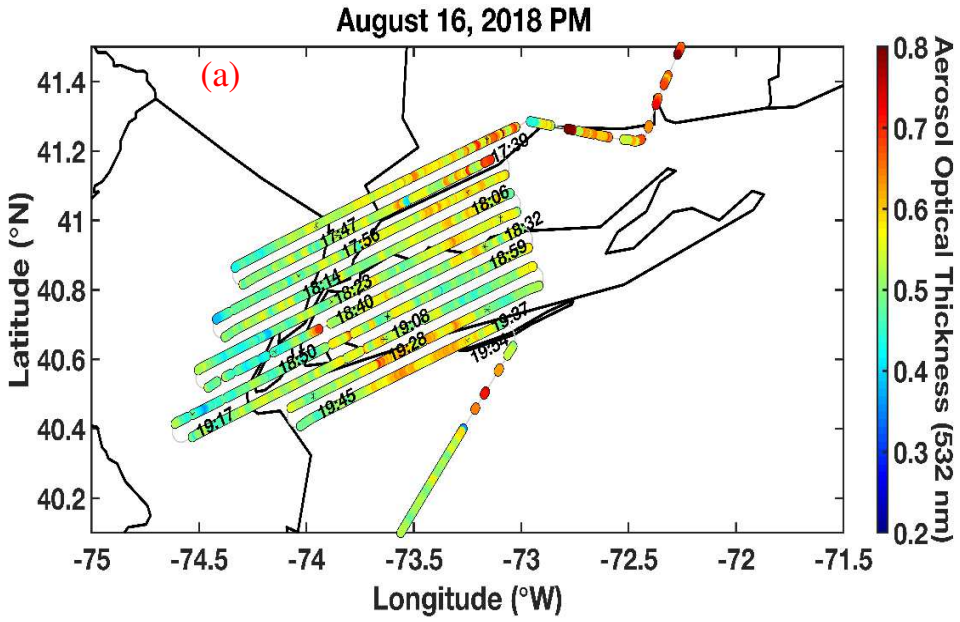

819

820 Fig.9 (a) NASA-airborne HALO-measured AOT along the flight tracks on Aug.16, 2018

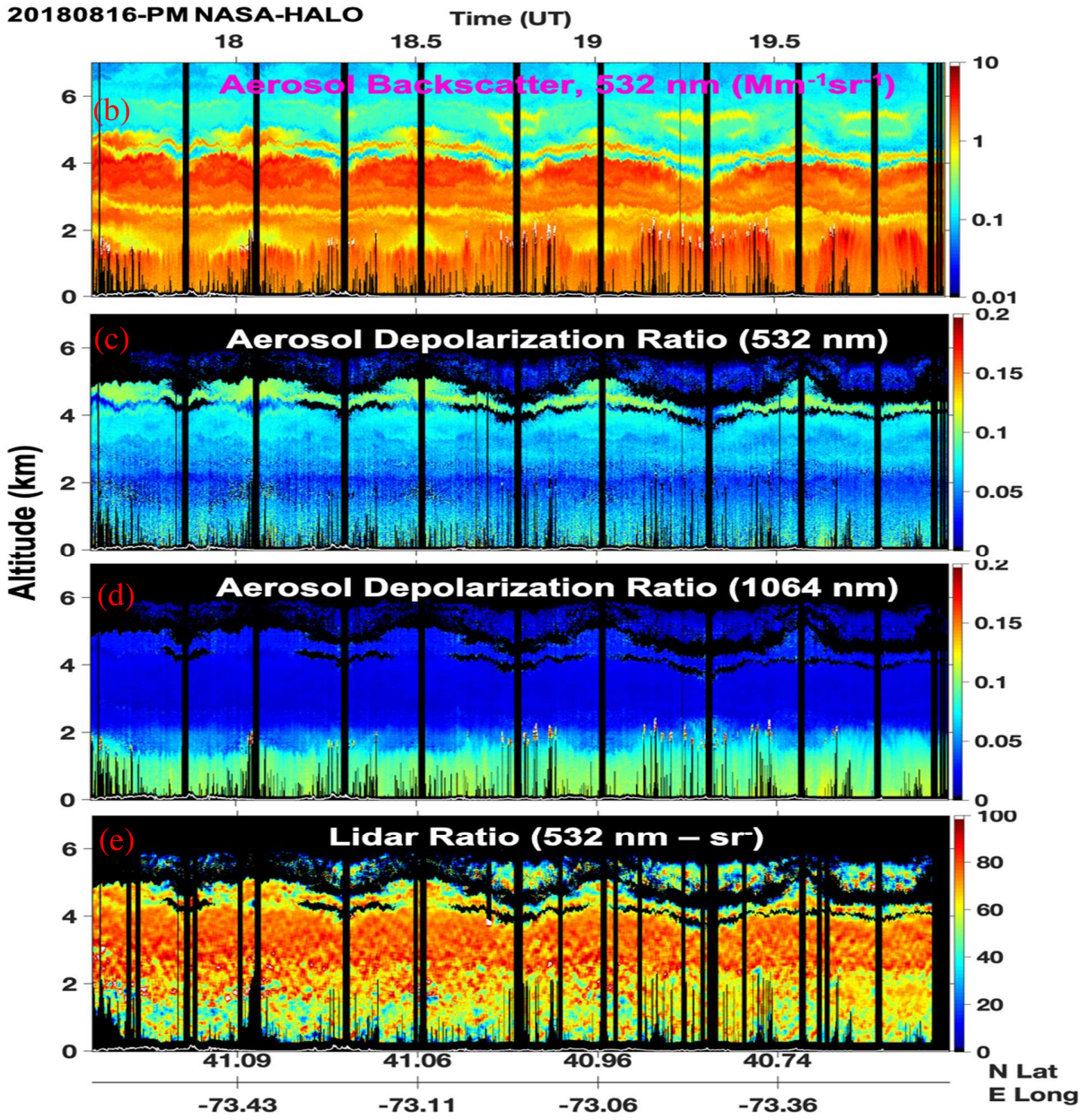

Fig.9 NASA-airborne HALO-measured aerosol backscatter coefficient (b), depolarization ratio (c-d) and lidar-ratio (e) on Aug.16, 2018 in the NYC and Long Island Sound area.

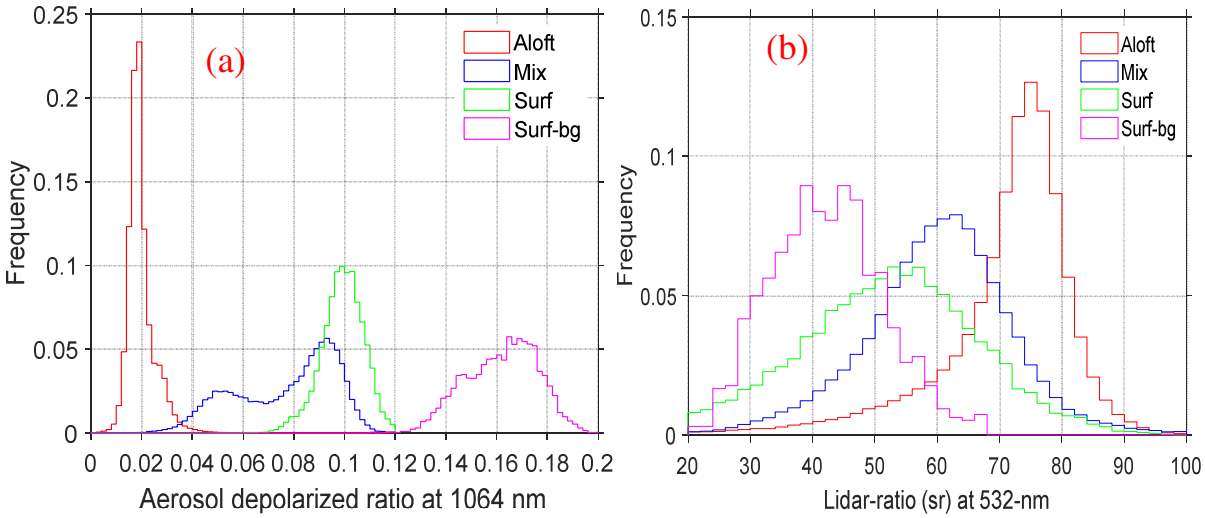

825

826 Fig.10 Histograms of aerosol depolarization ratio at 1064 nm (a) and lidar-ratio at 532-nm (b) at the
827 different altitudes measured by NASA airborne HALO on Aug.16, 2018 in NYC and Long Island Sound
828 area. Aloft: 2.5 – 4.7 km altitude; Mix: 0.5-1.5 km; Surf :< 0.5 km. Surf-bg: surface-background data
829 before the smoke intrusion at 9:00-11:00 EDT on Aug.15, 2018.

830

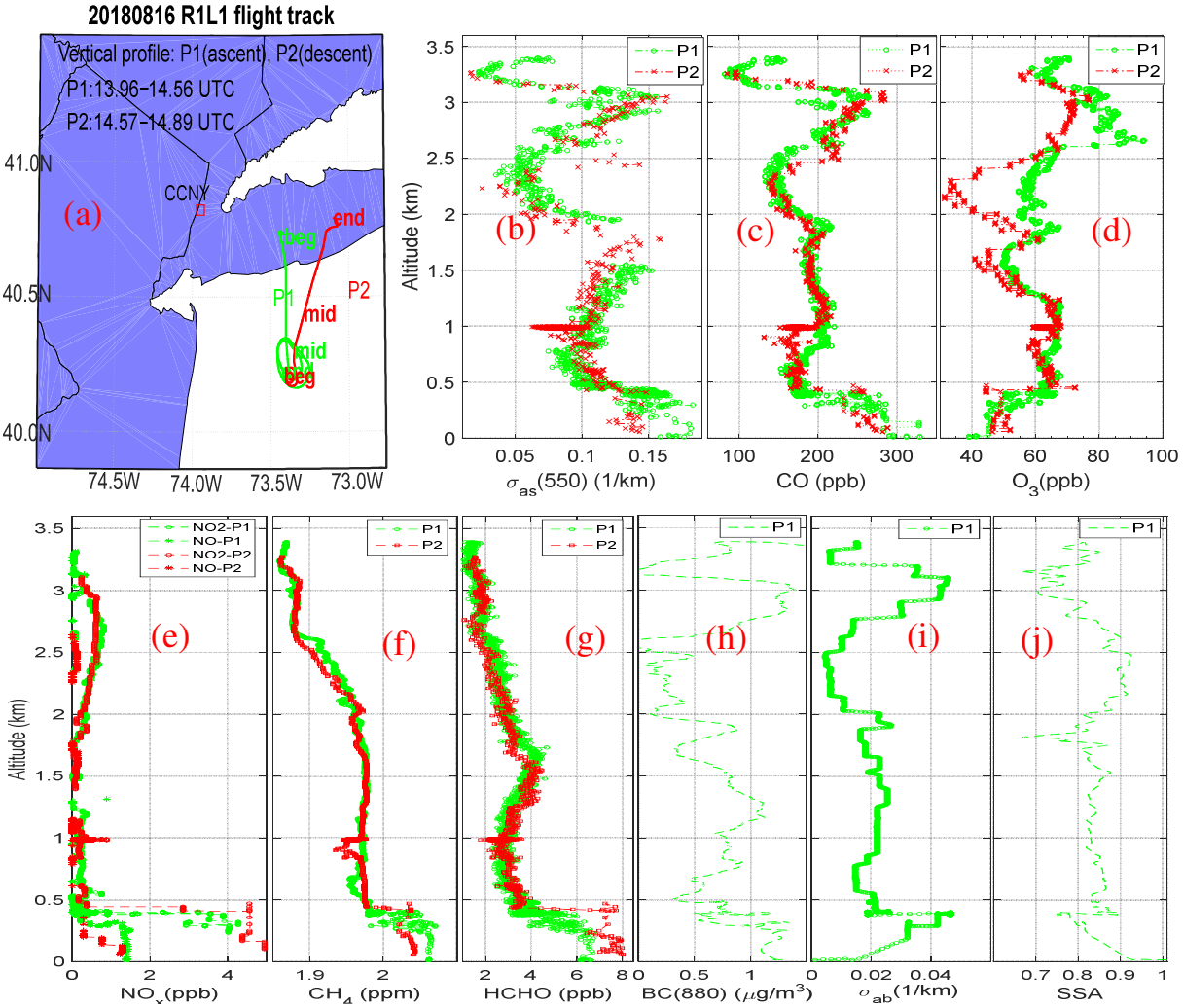

Fig.11. UMD aircraft flight tracks (a) and vertical distribution of aerosol total scattering (σ_{as}) (b), CO (c), O3 (d), NOx (e), CH4 (f), HCHO (g), BC (h), aerosol absorption (σ_{ab}) (i), and SSA (j) on Aug.16, 2018 (Vertical profile P1: Time=13.96-14.56 UTC or 9:58-10:34 EDT, Ascent; P2: Time=14.57-14.89 UTC or 10:34-10:53 EDT during the descent)

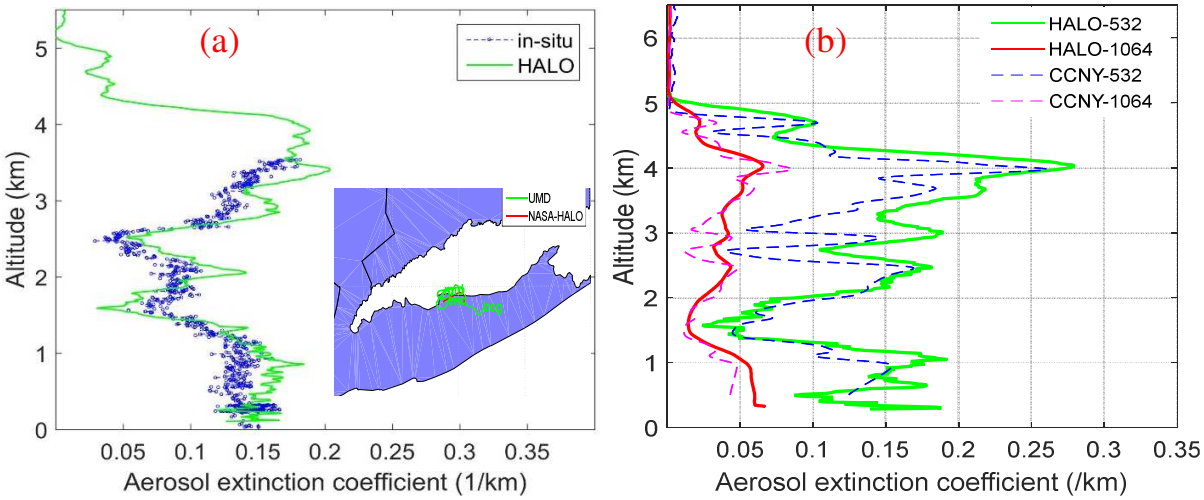

Fig. 12 Comparison of aerosol extinction profiles on Aug.16, 2018. (a) NASA-HALO vs. UMD aircraft in-situ at 19:56-20:23 UTC (15:56-16:23 EDT); (b) CCNY-lidar vs. HALO (HALO data <12 km from CCNY-site and CCNY-data within the 5-min from HALO overpass)

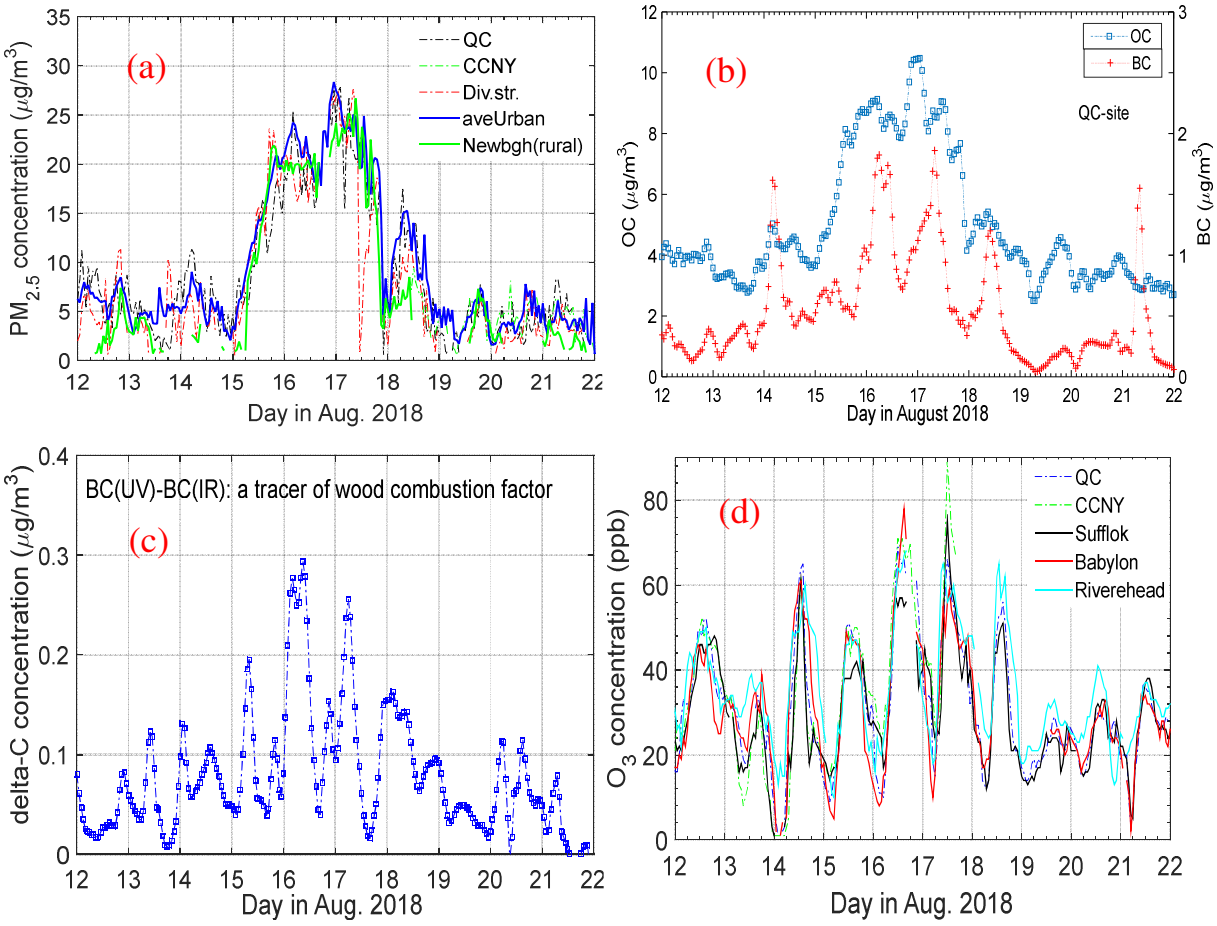

Fig.13 Temporal variation of ground $PM_{2.5}$ (a), OC and BC (b), delta-C (c) and O_3 (d) in the NYC area during Aug. 12-22, 2018.

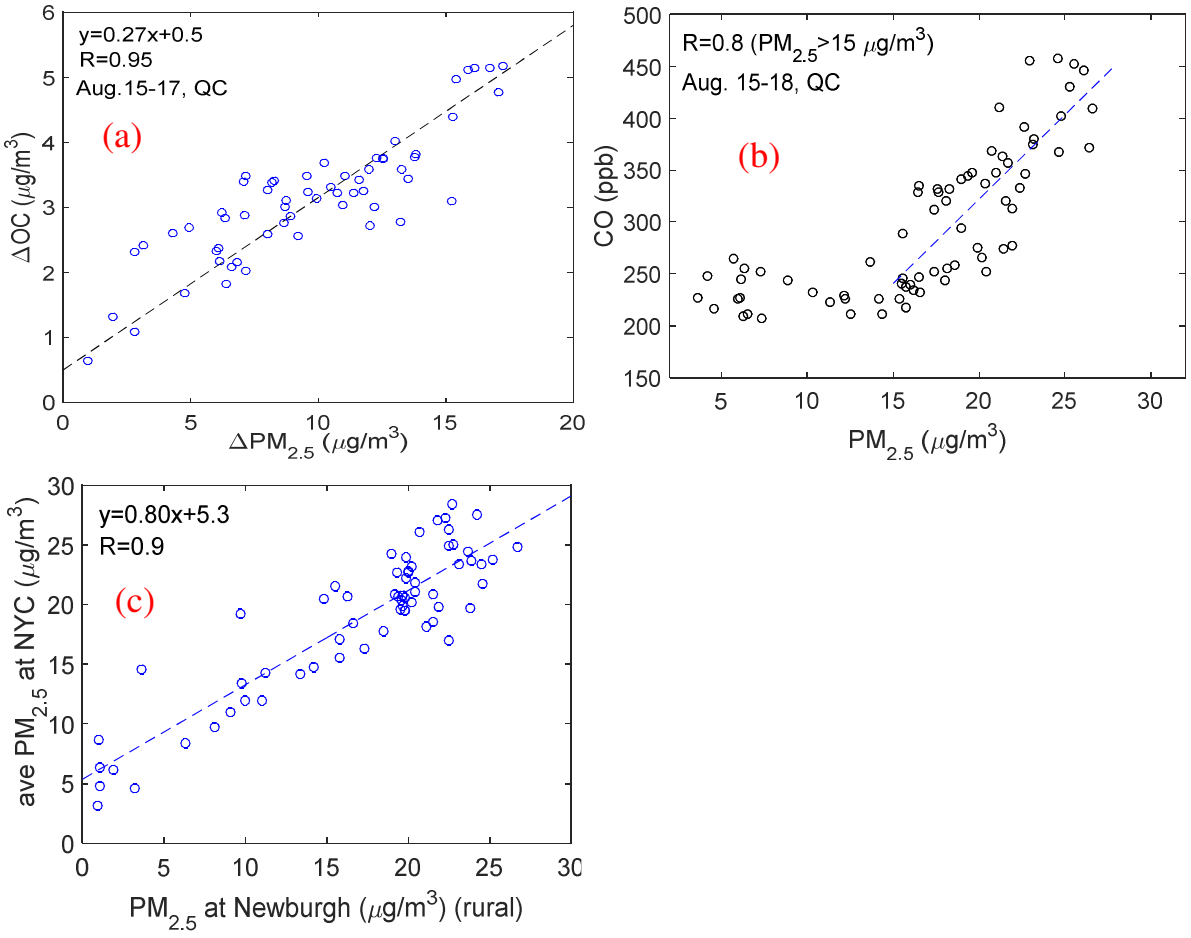

Fig.14 Correlation between the increment of OC and $PM_{2.5}$ (a), CO and $PM_{2.5}$ at QC-site (b), and $PM_{2.5}$ correlation at NYC urban and rural area (c) on Aug. 15-17, 2018.

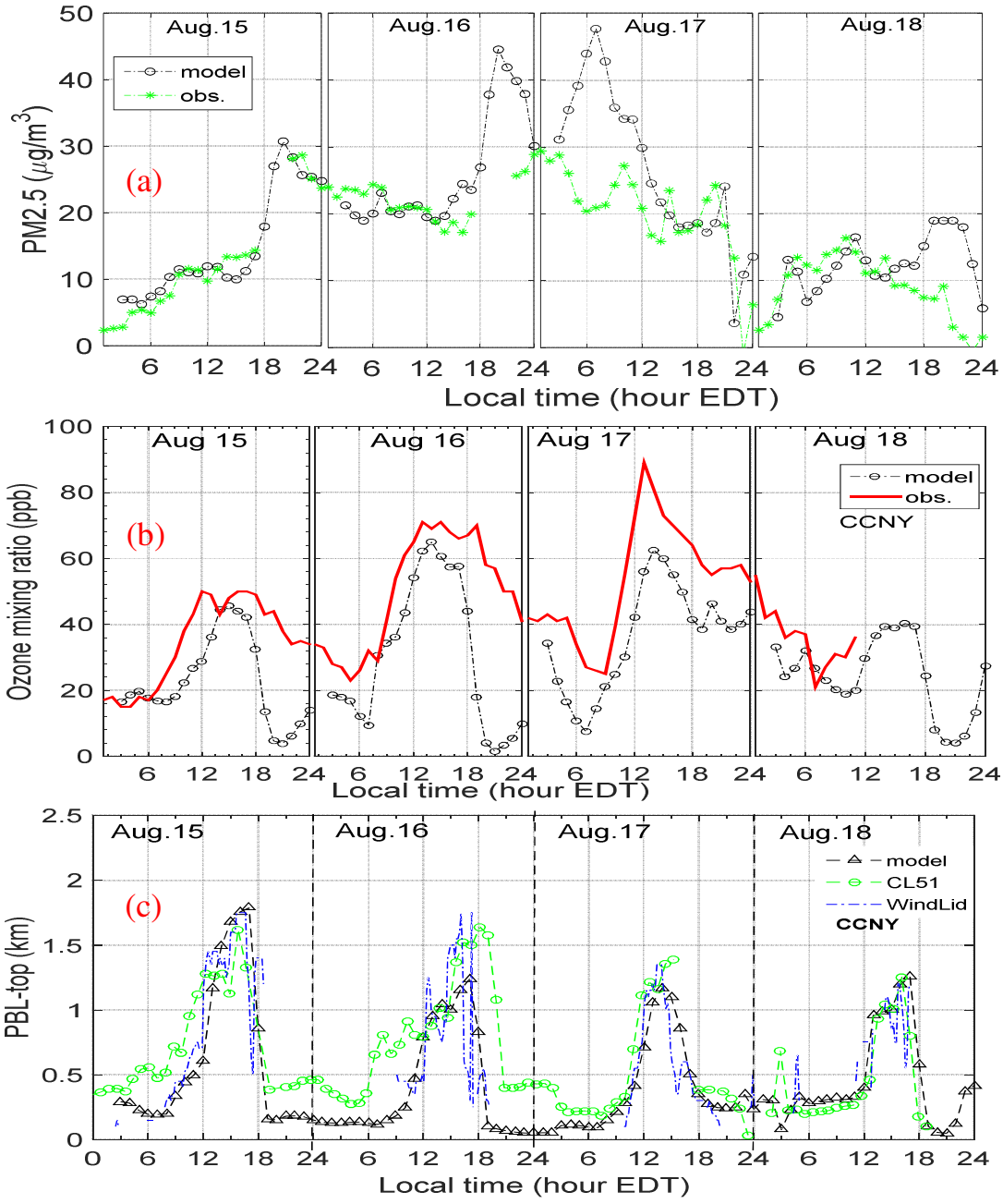

Fig.15 Comparison of ground $PM_{2.5}$ (a), O_3 (b) and PBLH (c) between the observations and model product.

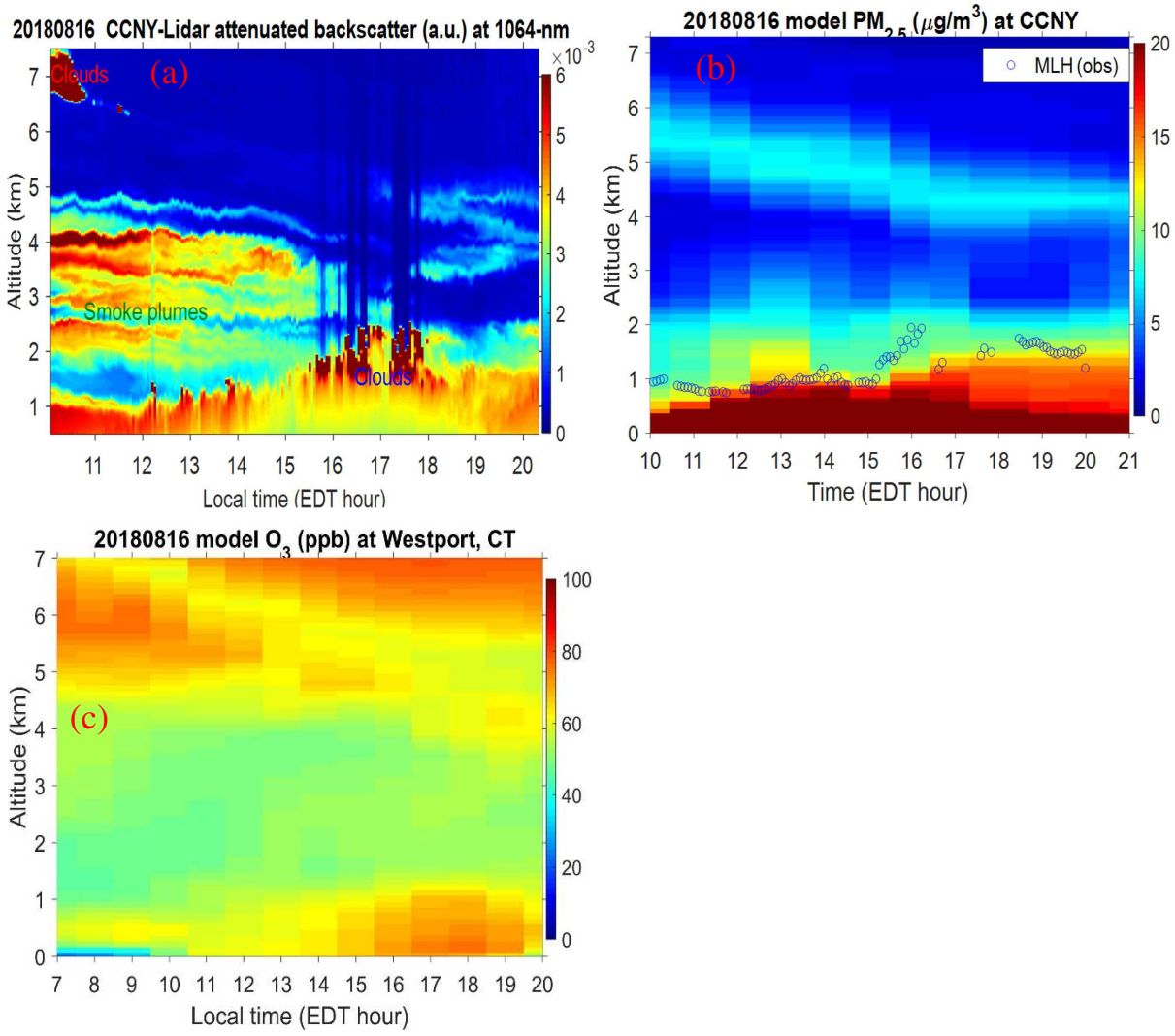

Fig. 16 Comparisons of aerosol ((a) and (b)) and O_3 (c) time-height cross-section between the observations and the NOAA-NAQFC simulations on Aug.16, 2018.

862 **Table-1. Ground site locations and the data used in this study ***

Site-name	Latitude (north,deg)	Longitude (west,deg)	Data used	Operator
NYBG	40.868	73.878	O_3	NYSDEC-AQS
IS-52	40.816	73.902	O_3	NYSDEC-AQS
CCNY	40.820	73.949	O_3,$PM_{2.5}$,CO, PBLH, aerosol extinction profile, AOD, Angstrom exponent	NYSDEC+CCNY
Division Street	40.715	73.995	$PM_{2.5}$	NYSDEC-AQS
Queens College (QC)	40.736	73.822	O_3,CO,$PM_{2.5}$, OC, BC	NYSDEC-AQS
Babylon	40.745	73.419	O_3	NYSDEC-AQS
Suffolk County	40.828	73.058	O_3	NYSDEC-AQS
Riverhead	40.961	72.712	O_3	NYSDEC-AQS
Newburgh	41.499	74.009	$PM_{2.5}$	NYSDEC-AQS
West Port	41.118	73.337	O_3 profile	NASA-LMOL
LMC(Bronx)	40.873	73.894	Wind profile	NYS-Mesonet
BNL	40.866	72.885	AOD, Angstrom exponent	AERONET-BNL

863 *The acronyms in Table-1 are spelled with full names in the contexts.

- Dense wildfire smoke mixing into PBL, and concurrent high ozone (>70 ppb) and CO in the plume layers.
- Smoke particles and urban aerosols show different spectral behavior (particle depolarization ratio at 1064 nm and lidar-ratio. Distinguish smoke particles from urban aerosols and identify their mixture in the PBL.